The Plant Cell, Vol. 25: 4596–4615, November 2013, www.plantcell.org

A BAR-Domain Protein SH3P2, Which Binds to Phosphatidylinositol 3-Phosphate and ATG8, Regulates Autophagosome Formation in *Arabidopsis*[C][W]

Xiaohong Zhuang,[a,1] Hao Wang,[a,1] Sheung Kwan Lam,[b] Caiji Gao,[a] Xiangfeng Wang,[a] Yi Cai,[a,2] and Liwen Jiang[a,c,3]

[a] School of Life Sciences, Centre for Cell and Developmental Biology and State Key Laboratory of Agrobiotechnology, The Chinese University of Hong Kong, Shatin, New Territories, Hong Kong, China

[b] Department of Molecular and Cell Biology, University of California, Berkeley, California 94720-3202

[c] The Chinese University of Hong Kong Shenzhen Research Institute, Shenzhen 518057, China

ORCID ID: 0000-0002-2480-8210 (X.Z.).

Autophagy is a well-defined catabolic mechanism whereby cytoplasmic materials are engulfed into a structure termed the autophagosome. In plants, little is known about the underlying mechanism of autophagosome formation. In this study, we report that SH3 DOMAIN-CONTAINING PROTEIN2 (SH3P2), a Bin-Amphiphysin-Rvs domain–containing protein, translocates to the phagophore assembly site/preautophagosome structure (PAS) upon autophagy induction and actively participates in the membrane deformation process. Using the SH3P2–green fluorescent protein fusion as a reporter, we found that the PAS develops from a cup-shaped isolation membranes or endoplasmic reticulum–derived omegasome-like structures. Using an inducible RNA interference (RNAi) approach, we show that RNAi knockdown of SH3P2 is developmentally lethal and significantly suppresses autophagosome formation. An in vitro membrane/lipid binding assay demonstrates that SH3P2 is a membrane-associated protein that binds to phosphatidylinositol 3-phosphate. SH3P2 may facilitate membrane expansion or maturation in coordination with the phosphatidylinositol 3-kinase (PI3K) complex during autophagy, as SH3P2 promotes PI3K foci formation, while PI3K inhibitor treatment inhibits SH3P2 from translocating to autophagosomes. Further interaction analysis shows that SH3P2 associates with the PI3K complex and interacts with ATG8s in *Arabidopsis thaliana*, whereby SH3P2 may mediate autophagy. Thus, our study has identified SH3P2 as a novel regulator of autophagy and provided a conserved model for autophagosome biogenesis in *Arabidopsis*.

INTRODUCTION

Macroautophagy (hereafter referred to as autophagy) plays an essential role in protein and organelle quality control and protects cells against pathogen infection or other unfavorable conditions. During this process, a structure termed the autophagosome engulfs and delivers cargo(s) into the lysosome/vacuole for degradation and recycling. In most cases, the autophagosome is initiated from the phagophore assembly site/preautophagosome structure (PAS), which then expands and seals the cargo(s) into a completed double-membrane structure (Xie and Klionsky, 2007; Mizushima et al., 2011).

Together with the identification of a number of autophagy-related genes (ATGs) in yeast (*Saccharomyces cerevisiae*) and mammalian cells, the analysis of autophagy-defective mutants has revealed several striking physiological roles of autophagy at both cellular and organismic levels, such as cellular renovation and tissue homeostasis (Mizushima and Komatsu, 2011). Among these, the machinery required for autophagosome formation is constituted by several core complexes: the ATG1/Unc-51-like kinase complex, the phosphoinositide 3-kinase (PI3K) complex, the Atg9 reservoir and its trafficking machinery, and two ubiquitin-like conjugation systems, including Atg12 and Atg8 (Xie and Klionsky, 2007; Mizushima et al., 2011)

Despite tremendous progress made in our understanding of the molecular mechanisms underlying autophagic pathways in yeast and mammals, autophagy studies in plants are still in their infancy. Although most of the ATG genes required for autophagy have been identified in plants (Avin-Wittenberg et al., 2012; Liu and Bassham, 2012), the molecular mechanism whereby ATG proteins regulate autophagosome formation in plant cells remains to be examined. Models for plant autophagosome formation are primarily deduced from those in yeast or mammals and are poorly characterized (Thompson and Vierstra, 2005; Li and Vierstra, 2012; Liu and Bassham, 2012). However, the identity of nascent autophagosome structures such as PAS is pivotal to several crucial questions regarding autophagosome biogenesis, including the membrane deformation mechanism and the origin of the autophagosome membrane. Membrane sources, including the endoplasmic reticulum (ER), mitochondria, ER-mitochondria contact sites, ER-Golgi intermediate compartment, Golgi apparatus,

[1] These authors contributed equally to this work.

[2] Current address: Department of Molecular Biology and Centre for Computational and Integrative Biology, Massachusetts General Hospital, and Department of Genetics, Harvard Medical School, Boston, MA 02114.

[3] Address correspondence to ljiang@cuhk.edu.hk.

The author responsible for distribution of materials integral to the findings presented in this article in accordance with the policy described in the Instructions for Authors (www.plantcell.org) is: Liwen Jiang (ljiang@cuhk.edu.hk).

[C] Some figures in this article are displayed in color online but in black and white in the print edition.

[W] Online version contains Web-only data.

www.plantcell.org/cgi/doi/10.1105/tpc.113.118307

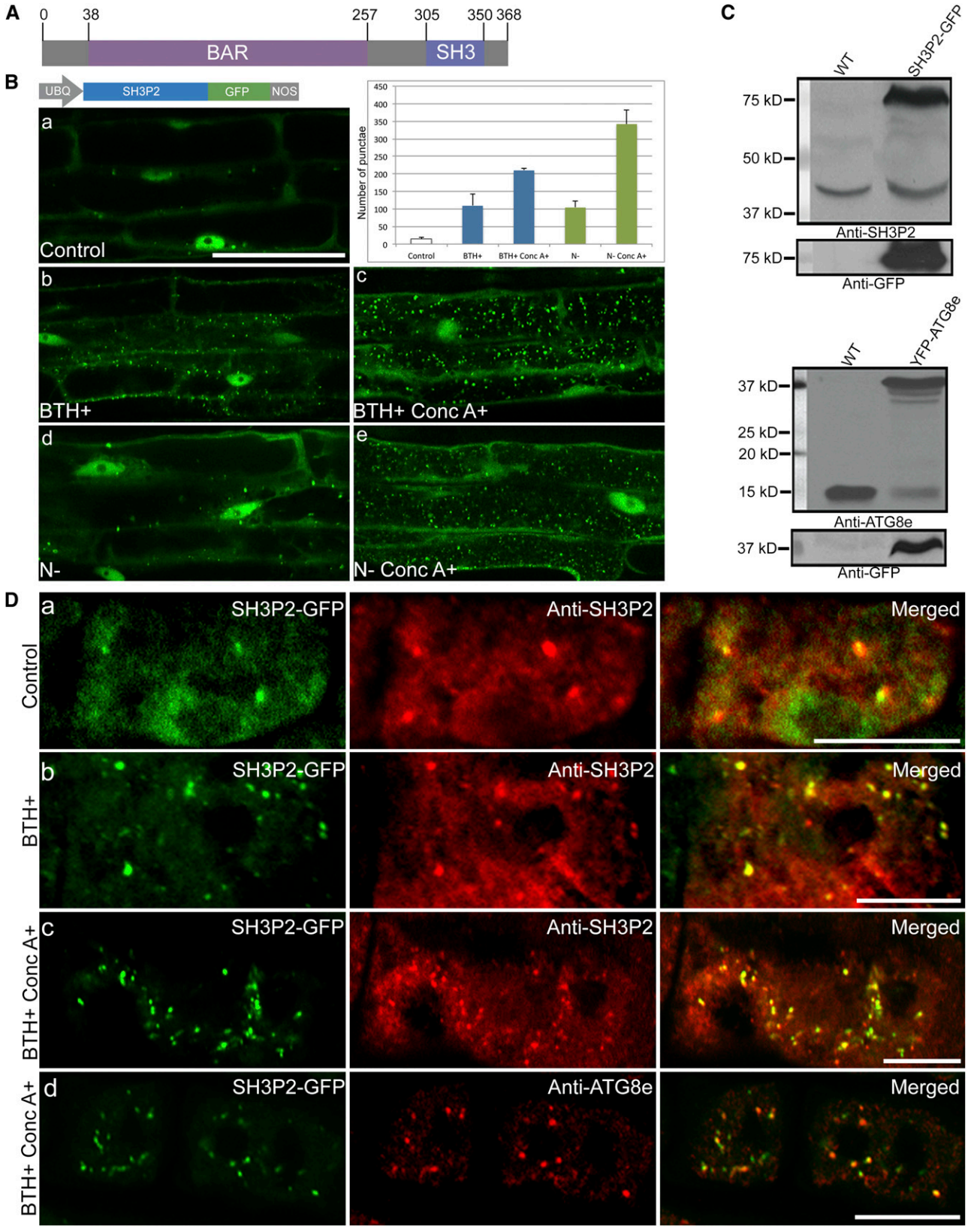

Figure 1. SH3P2-GFP Responds to Autophagy Induction.

and plasma membrane have been postulated to contribute to autophagosome formation in yeast and/or mammalian cells (Axe et al., 2008; Hayashi-Nishino et al., 2010a, 2010b; Hailey et al., 2010; Noda et al., 2011; Ohashi and Munro, 2010; Ravikumar et al., 2010; Ge et al., 2013; Hamasaki et al., 2013). In plants, however, most observations of autophagosome-related structures have been based on the classical features of autophagosomes: their isolated double-membrane appearance, enclosed autophagic cargos, and labeling with an autophagosome marker (Rose et al., 2006; Toyooka et al., 2006; Katsiarimpa et al., 2011; Takatsuka et al., 2011; Hanamata et al., 2012). So far, only one electron microscopy (EM) study has shown direct labeling of a double-membrane autophagosome structure in *Arabidopsis thaliana* with antibodies against the autophagosomal marker ATG8 (Reyes et al., 2011). Despite this single study, investigations on autophagosome biogenesis in plants have yet to reveal the detailed steps involved in this process and well defined intermediate structures.

A complicated situation for autophagy studies in plants is the great expansion of the ATG subfamily. For example, *Arabidopsis* possesses nine isoforms of ATG8 and eight homologs for ATG18 (Avin-Wittenberg et al., 2012; Liu and Bassham, 2012). On the other hand, key players, such as ATG14 and Bax-interacting factor1 (Bif-1; also known as Endophilin B1), have been identified as residing on/near PAS, where they mediate membrane deformation in cooperation with the PI3K complex (Takahashi et al., 2007; Matsunaga et al., 2010). However, orthologs of these membrane-remodeling regulators have not been identified in plants. Owing to their fundamental roles during autophagosome formation in eukaryotic cells, the question arises as to what the driving force for membrane remodeling is during autophagosome formation in plant cells. Accordingly, we urgently need a reliable map of autophagosome formation in plants, and we need to identify the corresponding regulator(s) of the equivalent steps in autophagosome formation.

In this study, we demonstrated that a novel non-ATG protein, SH3 DOMAIN-CONTAINING PROTEIN2 (SH3P2), which belongs to the Bin-Amphiphysin-Rvs (BAR) domain–containing protein family, plays an essential role in autophagy in *Arabidopsis*. Upon induction of autophagy, a pronounced relocalization of SH3P2 onto the autophagosome membrane was observed, as evidenced by autophagosome markers and structural features. Using SH3P2 as a probe, we characterized autophagosome-related structures, including the isolation membrane and ER-derived omegasome-like structures, thus extending the conserved model of autophagosome morphological progression to plants. To examine the role of SH3P2, we generated RNA interference (RNAi) knockdown transgenic plants, which showed defects in both development and autophagy. Further in vitro liposome/lipid binding assays demonstrate that SH3P2 possesses membrane-binding ability and specifically binds to phosphatidylinositol 3-phosphate (PI3P). Particularly, SH3P2 is shown to associate with the PI3K complex to facilitate autophagosome formation because SH3P2 promotes PI3K foci formation, while wortmannin (a PI3K inhibitor) treatment inhibits SH3P2 from translocating to autophagosomes. Moreover, SH3P2 interacts with ATG8s through its SH3 domain.

RESULTS

Green Fluorescent Protein-Tagged SH3P2 Responds to Autophagy Induction

Previous studies identified three SH3 domain–containing proteins in *Arabidopsis*: SH3P1, SH3P2, and SH3P3 (Lam et al., 2001, 2002). Structural analysis revealed that the three proteins also contain an N-terminal BAR domain. Such structural features are found in endophilins, a well-known membrane-associated protein family that actively participates in clathrin-dependent endocytosis (Dawson et al., 2006). Sequence alignment analysis revealed that SH3P2 shares significant similarities to SH3P1 and SH3P3, with amino acid identities of 43 and 53%, respectively (see Supplemental Figure 1A online). However, SH3P1 and SH3P3, but not SH3P2, have been reported to interact with endocytic partners (Lam et al., 2001, 2002), indicating that SH3P2 might function in other pathway(s). Interestingly, in mammalian cells, Bif-1, in contrast with other endophilin subfamily members, has been shown to play a role in autophagy (Takahashi et al., 2007, 2011, 2013).

To test for a possible role of SH3P2 in autophagy in plants, we first generated transgenic *Arabidopsis* plants expressing green fluorescent protein-tagged SH3P2 (SH3P2-GFP) driven by a ubiquitin (UBQ) promoter and examined the subcellular distribution of SH3P2-GFP after autophagy induction. Benzo-(1,2,3)-thiadiazole-7-carbothioic acid *S*-methyl ester (BTH), a salicylic acid agonist that triggers the autophagic pathway in *Arabidopsis* (Yoshimoto et al., 2009; Wang et al., 2011), was applied to transgenic SH3P2-GFP plants. As shown in Figure 1Bb, SH3P2-GFP

Figure 1. (continued).

(A) Schematic domain structure of SH3P2. SH3P2 contains an N-terminal BAR domain (38 to 257 amino acids), and a C-terminal SH3 domain (305 to 350 amino acids). Numbers represent amino acid positions, starting at the N terminus.

(B) Propagation of SH3P2-GFP punctae after autophagy induction. Top panel shows the chimeric DNA construct used to generating transgenic plants. Middle panel, roots of 5-d-old seedlings expressing SH3P2-GFP were transferred to MS medium (Control) **(a)**, MS medium with BTH (100 μM) for 8 h **(b)**, MS medium BTH (100 μM) and Conc A (0.5 μM) for 8 h **(c)**, MS medium without nitrogen for 48 h **(d)**, and MS medium without nitrogen for 36 h and an additional 12 h with a combination of Conc A treatment **(e)**. The number of autophagosome-related punctae per root section from different treatments was quantified and is shown in the top, right panel. The results were obtained from three independent experiments (error bars ± SD). Bars = 50 μm.

(C) Immunoblot analysis with SH3P2 and ATG8e antibodies. Both antibodies recognize the endogenous proteins in wild-type (WT) and transgenic plants respectively.

(D) Confocal microscopy images of SH3P2-positive organelles labeled with antibodies against SH3P2 (**[a]** to **[c]**) and ATG8e **(d)** in transgenic plants. Bars = 10 μm.

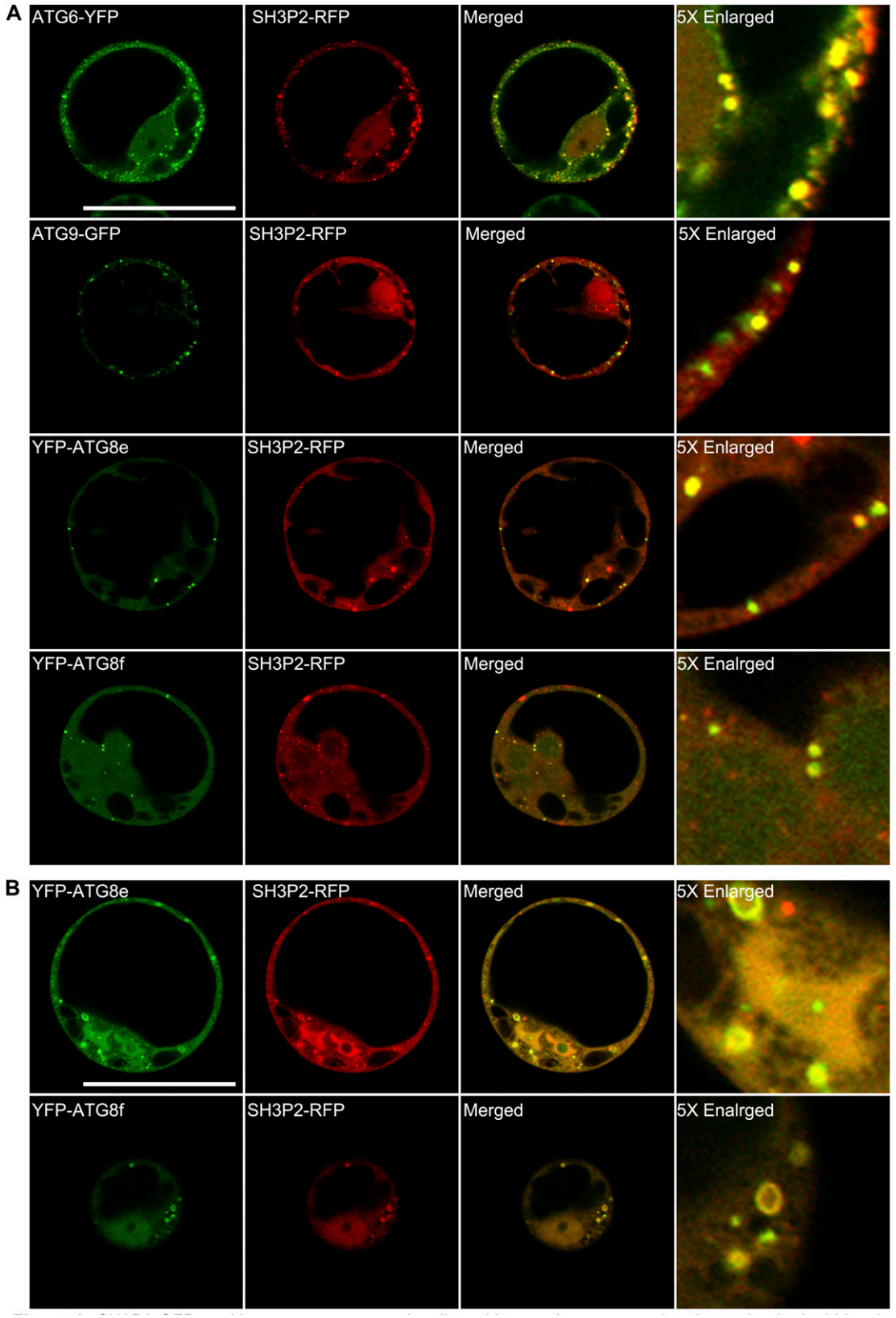

Figure 2. SH3P2-GFP–Positive Compartments Colocalize with Autophagosome-Related Proteins in *Arabidopsis* PSBD Protoplasts.

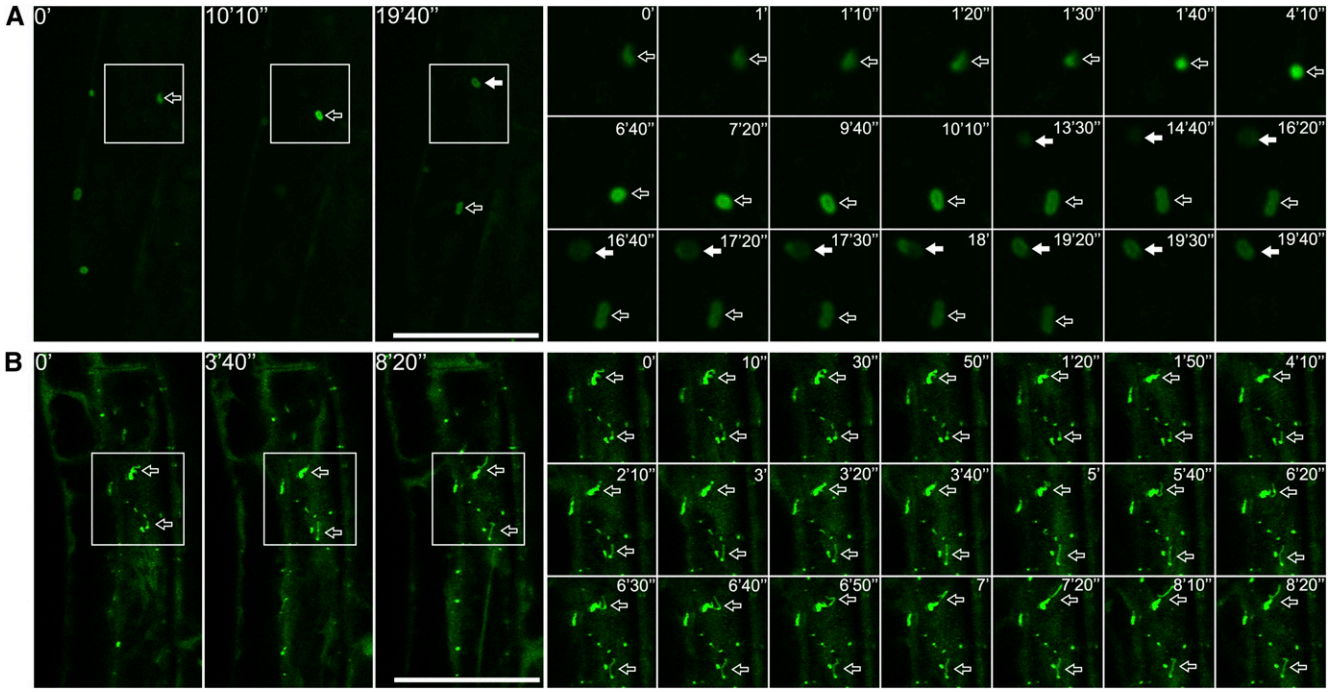

Figure 3. Dynamics of the SH3P2-GFP–Positive Structures Reveal Autophagosome Formation.

Roots of 5-d-old seedlings expressing SH3P2-GFP were transferred to MS with BTH (100 μM) for 8 h and observed using spinning disk microscopy **(A)** or confocal microscopy **(B).** Bars = 50 μm.

(A) Time-lapse imaging of autophagosome formation in SH3P2-GFP transgenic root cells. Three representative images, indicating beginning (0 min), middle (10 min 10 s), and last (19 min 20 s) frames, are shown on the left. The region in the white box was enlarged and shown on the right. Open arrow indicates the isolation membrane that extended from 0 min and formed a large ring-like structure after ~4 min. Closed arrow indicates another ring-like structure formed from ~13 min 30 s. See also Supplemental Movie 1 online for the full time-lapse series.

(B) Dynamics of SH3P2-GFP–positive tubular structures. Three representative images, indicating beginning (0 min), middle (3 min 40 s), and last (8 min 20 s) frames, are shown on the left. Arrows indicated two tubular structures labeled by SH3P2-GFP. Time-lapse sequences of enlargements of the indicated region are shown on the right. See also Supplemental Movie 2 online for the full time-lapse series.

[See online article for color version of this figure].

largely translocated from the cytosol (Figure 1Ba) to numerous punctate compartments after 8 h of BTH treatment. In addition, treatment with Concanamycin A (Conc A), a V-ATPase inhibitor, greatly increased the number of SH3P2-GFP punctae in the vacuole (Figure 1Bc). Since Conc A treatment leads to vacuole deacidification and prevents the degradation of autophagic bodies in the vacuole (Yoshimoto et al., 2004), these results indicate that SH3P2-GFP is in the autophagic pathway in *Arabidopsis*.

To confirm the autophagic response of SH3P2, we next tested if SH3P2-GFP is sensitive to N starvation, another well-defined condition for autophagy induction (Yoshimoto et al., 2004). Indeed, the population of SH3P2-GFP–positive compartments was greatly increased in transgenic SH3P2-GFP plants subjected to N starvation (Figure 1Bd) and even more when N starvation was combined with Conc A treatment (Figure 1Be). Further time-course analysis showed that autophagy induction by BTH is more pronounced than that of N starvation treatment (see Supplemental Figures 2A and 2B online). Taken together, these results demonstrate that SH3P2-GFP indeed lies on the autophagic pathway in *Arabidopsis*.

To find out if SH3P2-GFP functions as endogenous SH3P2 in autophagy in *Arabidopsis*, we next generated antibodies specific to SH3P2 and ATG8e, an accepted autophagosome marker in plants (Yoshimoto et al., 2004; Contento et al., 2005; Phillips et al., 2008; Wang et al., 2011). Immunoblot analysis using proteins isolated from either *Arabidopsis* wild-type or transgenic SH3P2-GFP or yellow fluorescent protein (YFP)–ATG8e plants showed that the SH3P2 and ATG8e antibodies specifically recognized the endogenous as well as the GFP fusion proteins (Figure 1C). In addition, ATG8e antibodies also recognized the ATG8f isoform (see Supplemental Figure 2C online). Further

Figure 2. (continued).

(A) SH3P2-RFP colocalized with ATG6-YFP, ATG9-GFP, and YFP-ATG8e and YFP-ATG8f when transiently expressed in *Arabidopsis* PSBD protoplasts.

(B) SH3P2-GFP is distributed on the autophagosome membrane. SH3P2-RFP ring-like structures overlapped with YFP-ATG8e and YFP-ATG8f signals. Bars = 50 μm.

immunofluorescent labeling studies using transgenic SH3P2-GFP plants showed that signals of SH3P2 antibody labeling were largely colocalized with SH3P2-GFP before or after BTH treatments (Figures 1Da to 1Dc), demonstrating the high specificity of the SH3P2 antibodies. Similarly, signals of ATG8e antibodies overlapped with those of YFP-ATG8e in YFP-ATG8e transgenic plants (see Supplemental Figure 3D online). In addition, in cells subjected autophagy induction, most of the SH3P2-GFP punctae colocalized with the immunofluorescent signals from ATG8e antibodies (Figure 1Dd), confirming that the SH3P2 punctae are indeed autophagosomes or related structures. Since the SH3P2 punctae did not fully overlap with the anti-ATG8e signals and ATG8e is believed to be a late/mature autophagosome marker, the distinct SH3P2 foci might represent autophagosome precursors. Such a scenario was therefore tested in the following experiments.

SH3P2-GFP Colocalizes with Autophagosome Markers

To verify the autophagosomal nature of the SH3P2-positive compartments, we performed colocalization studies using *Arabidopsis* protoplasts transiently coexpressing SH3P2-RFP (for red fluorescent protein) with several known components of core autophagy machinery. These included the PI3K complex (ATG6-YFP), ATG9 complex (ATG9-GFP), and ATG8 conjugate system (YFP-ATG8e and YFP-ATG8f) (Hanaoka et al., 2002; Yoshimoto et al., 2004; Fujiki et al., 2007). As shown in Figure 2A, ATG6-YFP and ATG9-GFP punctae largely colocalized with SH3P2-RFP, whereas the YFP-ATG8e and YFP-ATG8f dots only partially overlapped with SH3P2-RFP punctae. In addition, the dots and ring-like structures defined by both YFP-ATG8e and YFP-ATG8f perfectly overlapped with SH3P2-RFP, particularly on the membrane, but not in the lumen (Figure 2B), thus excluding the possibility that SH3P2-GFP is sequestered into the autophagosome lumen as cargo. By contrast, as shown in Supplemental Figure 3B online, SH3P2-GFP–positive punctae were distinct from most endomembrane organelle markers, including ManImannan endo-1,4-β-mannosidase1-RFP (Golgi apparatus), RFP-vacuolar sorting receptor (multivesicular body/prevacuolar compartment), and RFP-SYP61 (*trans*-Golgi network) (Tse et al., 2004; Lam et al., 2007; Cai et al., 2012). Taken together, these results demonstrate that both SH3P2 fusions and native SH3P2 proteins are characteristic of autophagosome-related structures in *Arabidopsis*.

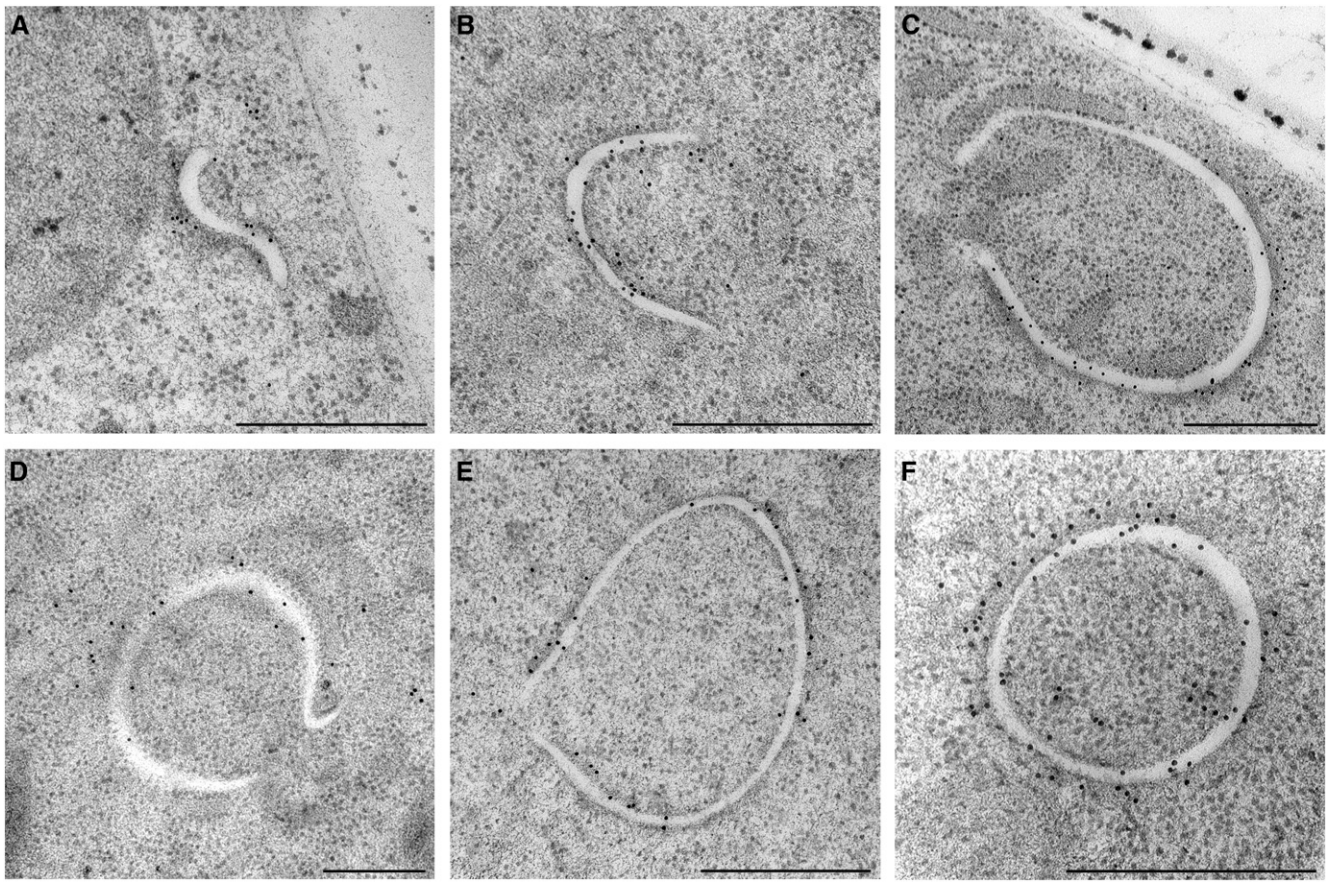

Figure 4. A Series of Images Showing Membrane Expansion and Cytosolic Sequestration of the SH3P2-Positive Structures Immunolabeled by SH3P2 Antibodies.
Bars = 500 nm.

SH3P2 Reveals the Structure and Dynamics of Autophagosomes

A general model for autophagosome formation in yeast and mammalian cells involves a series of morphological steps beginning with the initiation of PAS, expansion of the autophagosome membrane, maturation of the autophagosome by cargo sequestration, and completion of the double membrane (Xie and Klionsky, 2007). However, there are only limited evidences for this model in plant cells (Rose et al., 2006; Toyooka et al., 2006; Katsiarimpa et al., 2011; Takatsuka et al., 2011; Hanamata et al., 2012). SH3P2-GFP signals were shown to translocate onto the autophagosome

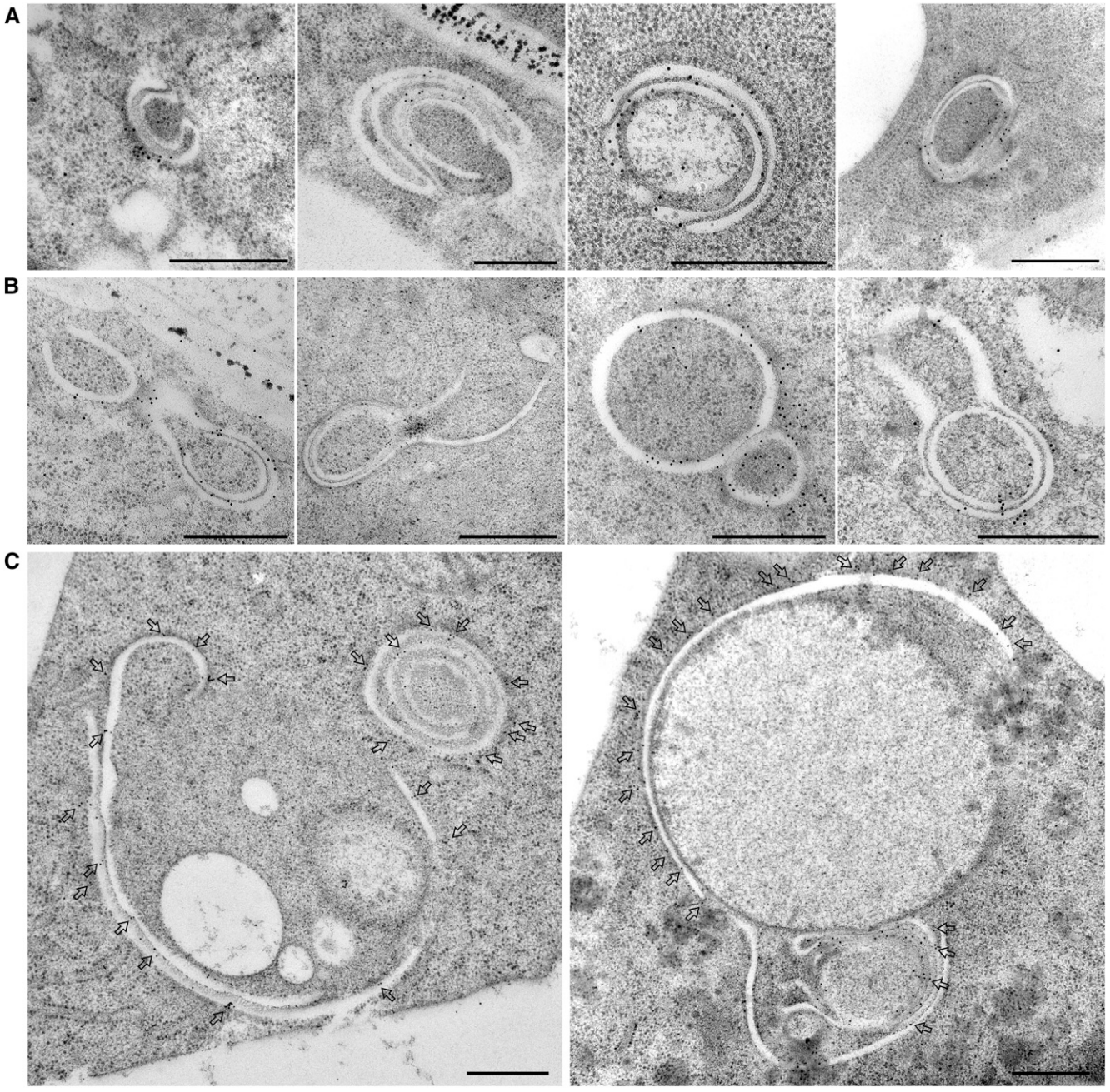

Figure 5. Multiple Steps Are Involved in the Formation of SH3P2-GFP–Positive Structures in Transgenic *Arabidopsis* Plants.

(A) Multilayer structures indicate autophagosome formation as labeled by antibodies against SH3P2.
(B) Examples show the fusion process of the SH3P2-positive organelles and amphisome-like structures labeled by SH3P2 antibodies.
(C) Examples show cargo sequestration during the maturation step. Arrows indicated the membrane distribution of SH3P2 labeled by the SH3P2 antibodies.
Bars = 500 nm.

membrane upon autophagy induction in *Arabidopsis* cells (Figures 1B and 2B), indicating its involvement in membrane progression of autophagosome formation. We thus hypothesized that the dynamics of SH3P2-positive structure formation in *Arabidopsis* generally reflects autophagosome biogenesis in plants, which can be observed and traced by time-lapse imaging of SH3P2-GFP in transgenic plants subjected to autophagy induction. Indeed, SH3P2-GFP first accumulated on a tubular-like structure (likely the isolation membrane) and gradually expanded into a cup-shaped structure at 1 min 30 s (Figure 3A, indicated by open arrow; see Supplemental Movie 1 online). After ~4 min, the isolation membrane sealed into a complete ring-like compartment, followed by the appearance of two ring-like structures at ~13 min 30 s. At the same time, another dot appeared (indicated by closed arrow), which ultimately form a ring-like structure. Interestingly, a protruding tail-like tube headed by a SH3P2-GFP spot was often observed

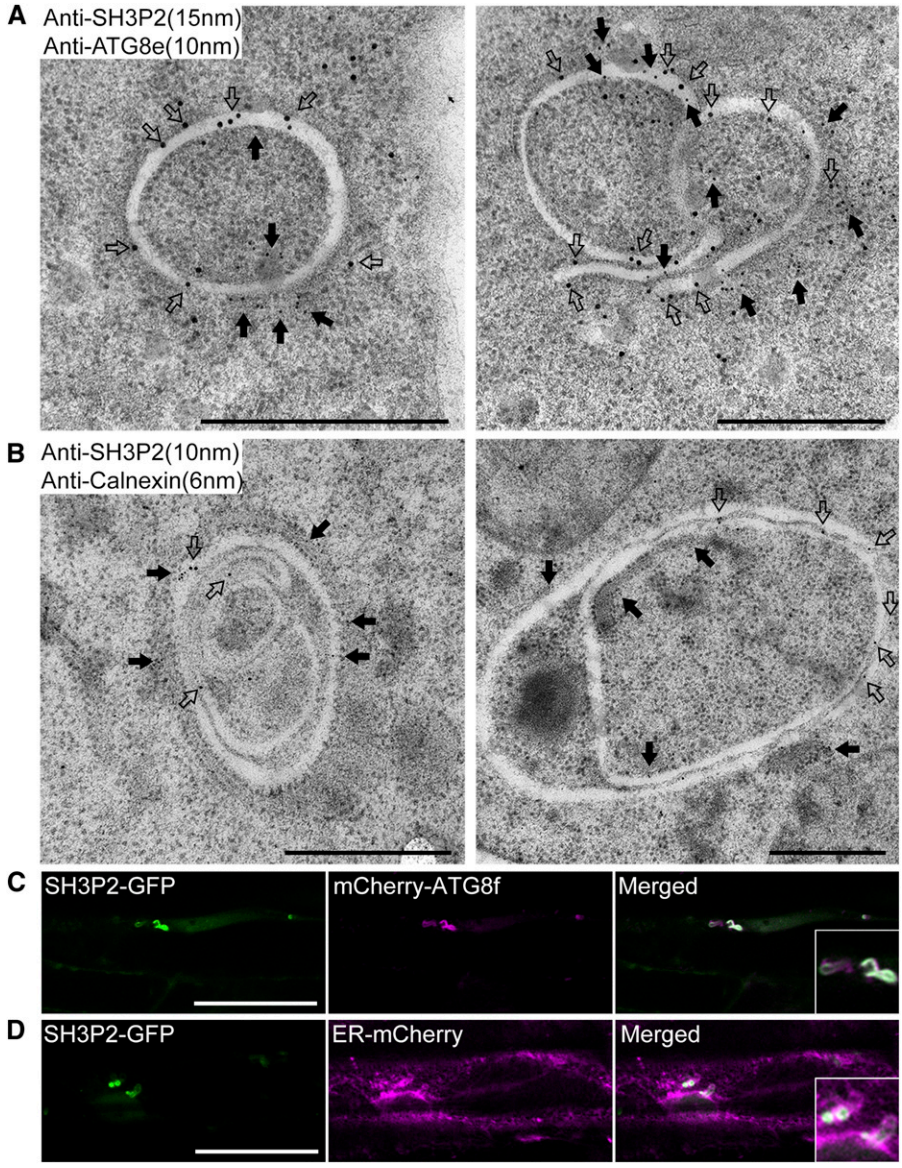

Figure 6. SH3P2-GFP–Containing Structures Were Positive with Autophagosome Marker and ER Marker.

(A) ATG8e antibodies (closed arrows) recognize SH3P2-positive organelles (open arrows). Bars = 500 nm.
(B) Antibodies against the ER marker calnexin (closed arrows) were detected along the membrane of SH3P2-positive (open arrows) organelles. Bars = 500 nm.
(C) Confocal images show the SH3P-GFP–positive compartments overlapping with the autophagosome membrane (mCherry-ATG8f) in transgenic a plant during autophagy. Bar = 50 μm.
(D) Confocal images show signals of ER-mCherry were in close proximity with SH3P-GFP–positive compartments, but were not in the lumen, during autophagy. Bar =50 μm.
[See online article for color version of this figure.]

(indicated by arrows) and likely represents developing autophagosomes for cargo sequestration (Figure 3B; see Supplemental Movie 2 online).

We next performed immunogold EM studies to elucidate the ultrastructure of SH3P2-GFP–positive compartments. Transgenic SH3P2-GFP *Arabidopsis* plants were first subjected to autophagy induction, followed by sample fixation processing via high-pressure freezing/freeze substitution and subsequent immunogold labeling using SH3P2 antibodies. Examples representing the autophagosome formation steps were identified: (1) the isolation membrane, (2) the cup-shape structure, (3) the encircling compartment, and (4) the completed double-membrane ring-like structure (Figure 4). The diameters of these SH3P2-positive structures ranged from 300 to 1000 nm, while SH3P2 predominantly localized to the membrane surfaces (Figure 4). Similar results were obtained using GFP antibodies (see Supplemental Figure 4A online).

SH3P2-positive structures with multiple membrane layers were also observed, which seemed to undergo a similar expansion and maturation process to form a multiple-layer compartment (Figure 5A). In addition, amphisome-like structures with fusion events were also found to be labeled by SH3P2 antibodies (Figure 5B). Interestingly, some of the SH3P2-positive structures were large and contained a long protruding membrane that engulfed organelle cargos (Figure 5C). We believe that these compartments correspond to the tubular structures observed under confocal microscopy (Figure 3B; see Supplemental Movie 2 online).

To verify that the SH3P2-labeled structures detected in *Arabidopsis* are indeed autophagosomes, we performed double-immunogold labeling using both SH3P2 and ATG8e antibodies in transgenic SH3P2-GFP plants after autophagy induction. As shown in Figure 6A, SH3P2 was predominantly detected on the membrane of the bi/multilayered structures, while ATG8e was dispersed. These results are consistent with the previous confocal observations (Figures 1Dd and 2B) and further support the notion that the SH3P2-GFP punctae were indeed autophagosomes or related structures. A consistent result was also obtained in double transgenic plants expressing SH3P2-GFP and a known autophagosome marker (mCherry-ATG8f). As shown in Figure 6C, after autophagy induction, the mCherry-ATG8f ring-like or tubular structures were seen to largely overlap with the SH3P2-GFP signals in the double transgenic plants. Taken together, these results confirm that SH3P2 translocates onto the autophagosome membrane during autophagy and defines a conserved autophagosome formation process in *Arabidopsis*.

In yeast and mammalian cells, an ER-derived and PI3P-enriched structure named the omegasome has been reported to contribute to the generation of the PAS (Axe et al., 2008; Noda et al., 2011). Interestingly, we also observed a proportion of the preautophagosomal structures exhibited ER fragments on both the outside and inside membrane surfaces (Figures 4C, 5Ab, and 5Ac). In some cases, isolation membranes labeled by SH3P2 seemed to be derived from the ER membrane with evident ribosomes (see Supplemental Figure 4B online). These observations were further supported by double immunogold labeling using Calnexin (ER marker) and SH3P2 antibodies, which showed their colocalization on the same autophagosome structures (Figure 6B). Consistently, in the SH3P2-GFP/ER-mCherry double transgenic plants, ring-like structures positively labeled by SH3P2-GFP were found to overlap largely with the ER-mCherry signals, proximally on the membrane, but not in the lumen during autophagy (Figure 6D). Since the ER network is the major source of membranes in the cell, plants might use the ER membrane as a platform for acute proliferation of autophagosomes. However, other membrane sources may be needed to generate the PAS because some of the SH3P2-GFP–positive autophagosome structures did not exhibit a direct connection to the ER (Figure 4).

SH3P2 Is Essential in Plant Development and Autophagy

We next used a loss-of-function approach to gain an insight into the role of SH3P2 in autophagy in *Arabidopsis*. We failed to obtain a T-DNA insertional knockout mutant of SH3P2. Alternatively, we employed a hairpin RNAi knockdown method to generate transgenic *Arabidopsis* plants expressing hairpin RNAi for SH3P2 under the control of the constitutive 35S promoter. Immunoblot analysis confirmed that this RNAi construct is specific for SH3P2 (Figure 7B; see Supplemental Figure 5B online). However, we

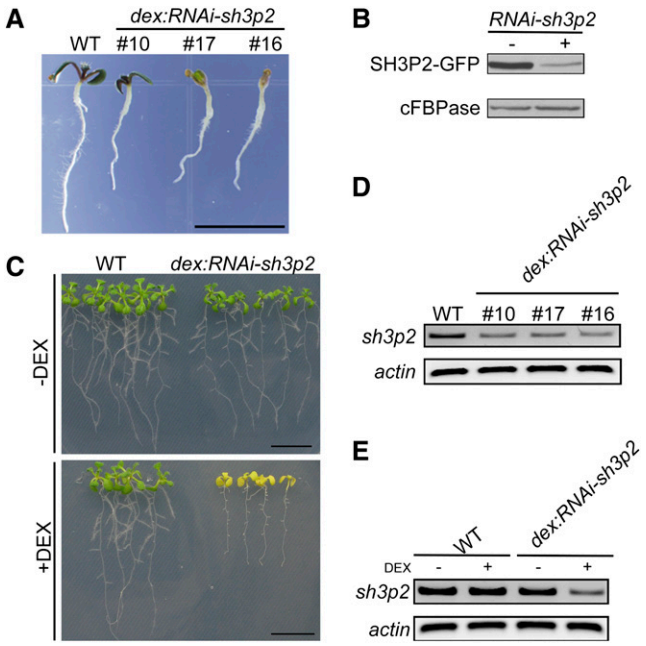

Figure 7. SH3P2 Is Indispensible during Plant Development.

(A) and **(D)** Phenotype of SH3P2 RNAi knockdown plants **(A)**. The wild type (WT) and three different lines of SH3P2 RNAi knockdown transgenic plants were grown on MS plates containing DEX for 7 d. Corresponding transcription levels were confirmed by RT-PCR analysis **(D)**. *Actin* transcripts are used as loading controls. Similar results were obtained from three independent experiments. Bar = 1 cm.

(B) Immunoblot characterization of the hairpin RNAi construct against SH3P2-GFP in *Arabidopsis* PSBD protoplasts.

(C) Downregulation of SH3P2 causes early leaf senescence and abnormal root growth. Wild-type and *dex:RNAi-sh3p2 Arabidopsis* plants were grown on MS plates for 7 d and followed with/without DEX treatment for another 7 d. Bars = 1 cm.

(E) Corresponding transcription levels were confirmed by RT-PCR analysis. *Actin* transcripts are used as loading controls.

[See online article for color version of this figure.]

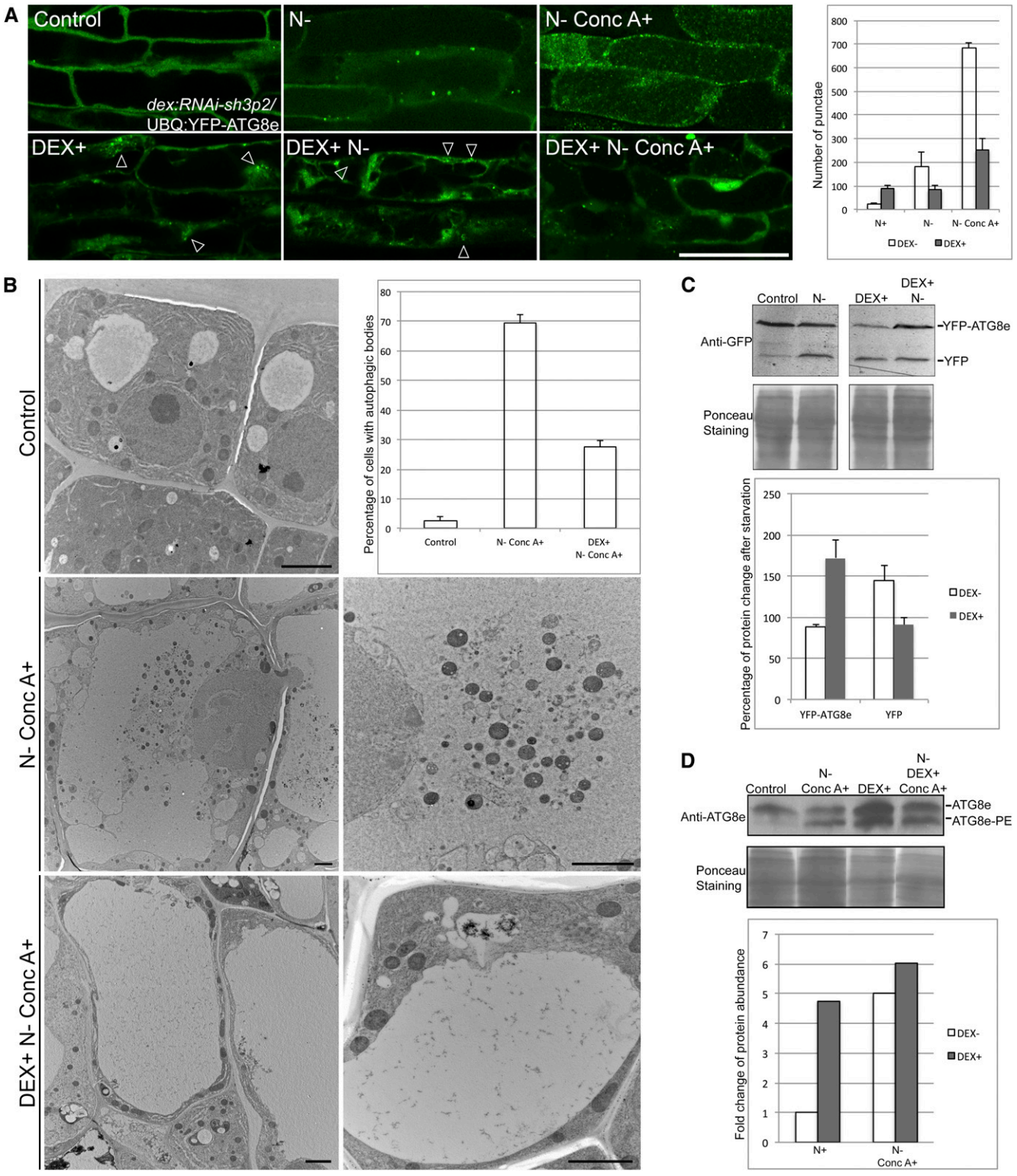

Figure 8. Autophagy Requires SH3P2 Activity in *Arabidopsis*.

Seven-d-old transgenic *Arabidopsis* plants were transferred to MS plates for 2 d, followed by N starvation for 1 d and an additional 12 h with or without a combination of Conc A treatment.

failed to obtain a SH3P2 RNAi knockdown plant under the control of the 35S promoter. Instead, we used the dexamethasone (DEX) inducible promoter to drive the hairpin RNAi fragment against SH3P2 and generated the *dex*:*RNAi-sh3p2* plants. When triggered with DEX, *dex*:*RNAi-sh3p2* plants were arrested soon after germination and exhibited abnormal root growth (Figure 7A). RT-PCR analysis confirmed that *sh3p2* transcription was downregulated upon DEX induction in transgenic plants (lines 10, 17, and 16) when compared with the wild type (Figure 7D).

Line 16 was used for testing the optimal silencing conditions for further examination in the SH3P2 knockdown background. Time-course tracing experiments showed that an abnormal phenotype in *dex*:*RNAi-sh3p2* started to appear from 2 d after DEX induction (see Supplemental Figure 5A online). RT-PCR analysis confirmed that the *sh3p2* transcription level was significantly downregulated after a 2-d DEX induction (Figure 7E). At day 14 after DEX induction, *dex*:*RNAi-sh3p2* plants exhibited early leaf senescence and abnormal root development, whereas the wild-type plants remained normal (Figure 7C). We thus used 7-d-old *dex*:*RNAi-sh3p2* seedlings 2 d after DEX induction for subsequent analyses.

To monitor the fate of autophagy in the SH3P2 knockdown background, we crossed the transgenic plant expressing the autophagosome marker (UBQ:YFP-ATG8e) with the *dex*:*RNAi-sh3p2* plant and induced autophagy with N starvation. As shown in Figure 8A, in the absence of DEX treatment, autophagy was induced, with the progressive detection of YFP-ATG8e punctae and enhanced YFP signal in the vacuole after N starvation, whereas additional Conc A treatment caused numerous autophagic bodies to accumulate. However, upon DEX induction, YFP-ATG8e degradation was suppressed during N starvation, with fewer autophagic bodies forming within the vacuole even in the presence of Conc A (Figure 8A, bottom panel). Consistent results were obtained in an EM analysis. As shown in Figure 8B, autophagic bodies accumulated within the vacuoles of cells subjected to N starvation and Conc A treatment, but not in control cells pretreated with DEX.

Immunoblot analysis was performed to measure the autophagic flux by examining the turnover ratio of YFP-ATG8e and free YFP. As shown in Figure 8C, when UBQ:YFP-ATG8e/*dex*:*RNAi-sh3p2* plants were subjected to N starvation without DEX induction, the amount of free YFP increased, whereas YFP-ATG8e decreased, which represents the normal processed degradation of autophagosomes in the vacuole. However, upon DEX induction, a significant delay in autophagy flux was detected, as indicated by the enhanced YFP-ATG8e signals, but without a significant increase in YFP signals (Figure 8C). In addition, small YFP-ATG8e positive punctae/tubules instead of ring-like structures accumulated within the cells after DEX induction (Figure 8A, arrowheads), suggesting that SH3P2 is not required for the recruitment of YFP-ATG8e to the autophagosome membrane.

To distinguish whether SH3P2 functions before or after the completion of autophagosome formation, we examined the ATG8 conversion rate in *dex*:*RNAi-sh3p2* plants using ATG8e antibodies (Mizushima et al., 2010; Suttangkakul et al., 2011). Generally, upon autophagy induction, an enhanced flux can be detected as the total amount of ATG8-PE is increased (representing the forming/completed autophagosomes), while the cytosolic ATG8 form decreases. Surprisingly, the expression levels of ATG8e-PE and ATG8e were remarkably increased after the suppression of SH3P2 (Figure 8D), implying that autophagosome expansion and/or maturation step(s) may be impaired, in which ATG8-PE has already conjugated onto the autophagosome membrane but is unable to be completed or delivered into the vacuole. Similar results were obtained in identical experiments when BTH was used to induce autophagy (see Supplemental Figure 5C online). Therefore, it is likely that SH3P2 is required for the autophagosome expansion and/or maturation step(s).

SH3P2 Binds to PI3P and Coordinates with the PI3K Complex to Function in Autophagy

Since SH3P2 contains a BAR domain (Figure 1A), which is a well-known membrane-binding module for membrane deformation (Frost et al., 2009), we propose that SH3P2 binds to the autophagosome membrane by itself to facilitate the expansion or fusion of autophagosome. Therefore, we next performed an in vitro liposome binding assay to test its membrane-binding capability. Indeed, as shown in Figure 9A, His-maltose-binding protein (MBP)-SH3P2 recombinant proteins bind to liposomes, whereas the control His-MBP proteins showed little binding.

To determine which lipid SH3P2 binds to, we next performed an in vitro lipid binding assay. As shown in Figure 9B, SH3P2 recombinant proteins bind to phosphatidylinositol phosphates

Figure 8. (continued).

(A) Confocal analysis of the starvation response of YFP-ATG8e in UBQ:YFP-ATG8e/*dex-RNAi-sh3p2* root tip cells. The vacuolar delivery of YFP-ATG8e was significantly suppressed in a parallel experiment with DEX treatment (bottom panel). Note that small YFP-ATG8e punctae accumulated after DEX induction (arrowheads). The number of YFP-ATG8e punctae per root section from plants subjected to different treatments was quantified and shown in the right panel. The results were obtained from three independent experiments (error bars ± SD). Bar = 50 μm.

(B) EM analysis of autophagic bodies in UBQ:YFP-ATG8e/*dex-RNAi-sh3p2* root tip cells. An example showing the vacuole contents for the corresponding sample was enlarged in the right column. The number of cells (>50) with autophagic bodies in the vacuole were counted and quantified (top). The results were obtained from three different root sections (error bars ± SD). Bars = 2 μm.

(C) Immunoblot analysis of the degradation rate of YFP-ATG8e after N starvation with/without DEX pretreatment in UBQ:YFP-ATG8e/*dex-RNAi-sh3p2* transgenic plants. The percentage of protein change (YFP-ATG8e or YFP) compared with the control was quantified **(bottom)**. Error bars represent the SD from three independent immunoblot results.

(D) Immunoblot analysis for the effect of SH3P2 knockdown on both ATG8e and ATG8e-PE in *dex*:*RNAi-sh3p2* plants. The fold change of ATG8-PE was quantified **(bottom)**. Error bars represent the SD from three independent immunoblot results.

[See online article for color version of this figure.]

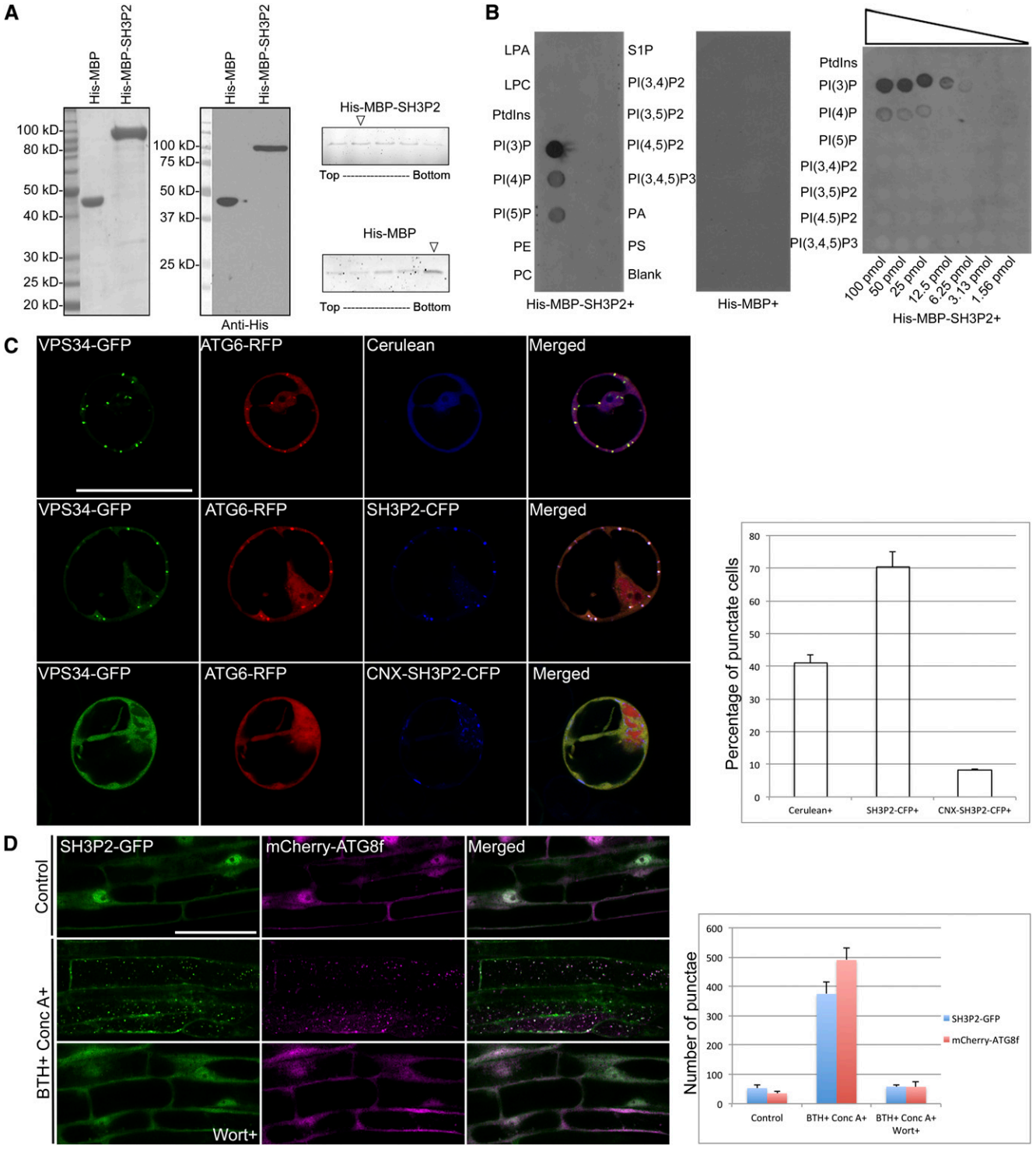

Figure 9. SH3P2 Binds to the Autophagosome Membrane in a PI3K-Dependent Manner.

(A) In vitro liposome binding assay showing the membrane binding ability of SH3P2. His-MBP-SH3P2 and His-MBP purified from *Escherichia coli* were analyzed by SDS-PAGE following Coomassie blue staining **(left)** and immunoblot with anti-His antibodies **(middle)**. Fractions from a liposome flotation assay using His-MBP-SH3P2 or His-MBP were analyzed by SDS-PAGE **(right)**. Arrow indicates the significant fractions with His-MBP-SH3P2 **(top)** or His-MBP **(bottom)**.

(B) Characterization of lipid binding ability of SH3P2 by PIP strips/array. LPA, Lysophosphatidic acid; LPC, Lysophosphocholine; PtdIns, Phosphatidylinositol; PtdIns(3)P, Phosphatidylinositol (3) phosphate; PtdIns(4)P; Phosphatidylinositol (4) phosphate; PtdIns(5)P, Phosphatidylinositol (5) phosphate; PE,

(PIPs), especially PI3P, whereas no signal was detected in the control with the His-MBP proteins. In addition, as shown in Supplemental Figure 6A, SH3P2-GFP–positive punctae largely overlap with the PI3P reporter (RFP-2XFYVE) (Helling et al., 2006; Vermeer et al., 2006; Thole et al., 2008; Zhang et al., 2011; Wang et al., 2013), further confirming that SH3P2 is able to bind to PI3P.

A conserved PI3K activity is essential for autophagy in plants, as silencing of ATG6 and VPS34 has been shown to limit cell death and reduce autophagosome formation in *Arabidopsis* and *Nicotiana benthamiana* plants (Liu et al., 2005; Fujiki et al., 2007; Patel and Dinesh-Kumar, 2008). When SH3P2-CFP (for cyan fluorescent protein) was coexpressed with VPS34-GFP and ATG6-RFP, we observed an enhanced production of VPS34- and ATG6-positive punctae that colocalized with SH3P2-CFP (Figure 9C). However, when SH3P2 was anchored onto the ER membrane by fusion with the ER retention signal of calnexin (daSilva et al., 2006; Niemes et al., 2010), the number of VPS34-GFP– and ATG6-RFP–positive punctae was significantly reduced (Figure 9C; see Supplemental Figure 6B online).

On the other hand, treatment with wortmannin, a PI3K inhibitor blocking autophagy (Blommaart et al., 1997; Takatsuka et al., 2004; Axe et al., 2008), resulted in a significant reduction of SH3P2-GFP and mCherryATG8f foci formation during autophagy, implying that SH3P2 is sensitive to wortmannin and requires PI3K activity to function in autophagy (Figure 9D).

SH3P2 Associates with the PI3K Complex and Interacts with ATG8

To better understand the molecular links between SH3P2 and the autophagy machinery, we searched for its interaction partner(s). Both yeast two-hybrid and immunoprecipitation assays showed that SH3P2 has a strong self-interaction via its BAR domain (Figures 10A to 10D), a result consistent with the known dimerization property of BAR domains (Dawson et al., 2006). Moreover, we showed that SH3P2 was immunoprecipitated with ATG6, while no significant interaction was detected in the yeast two-hybrid assay (Figures 10A and 10E). These results indicate that SH3P2 is associated with the PI3K complex via other potential mediator(s).

Interestingly, it was implied that SH3P2 interacts with ATG8f, based on the results of a yeast two-hybrid assay (Arabidopsis Interactome Mapping Consortium, 2011). Indeed, we showed that SH3P2 interacted with both ATG8f and ATG8e in our yeast two-hybrid assay (Figure 10A). These interactions were confirmed by an in vivo coimmunoprecipitation analysis using epitope-tagged SH3P2 and ATG8e or ATG8f, respectively (Figure 10E). In addition, endogenous SH3P2 was precipitated with YFP-ATG8e in transgenic *Arabidopsis* plants after autophagy induction (Figure 10F). Intriguingly, this interaction seems to be mediated by the SH3 domain of SH3P2 (Figure 10G).

DISCUSSION

SH3P2 Resides on PAS and Reveals Autophagosome Formation upon Autophagy Induction in *Arabidopsis*

In this study, we demonstrated that SH3P2, an N-terminal BAR-containing protein, was involved in autophagosome formation in *Arabidopsis*. So far, the morphological features and identities of autophagosomes and their dynamics have been investigated to a limited extent in plant cells when compared with yeast and mammals. Fluorescently tagged ATG8/LC3 or other ATG markers have been widely used as markers to monitor autophagy in yeast and other higher eukaryotes, including plants (Yoshimoto et al., 2004; Toyooka et al., 2006; Xie and Klionsky, 2007). However, structures that are necessary for autophagosome formation in plants have remained elusive. Double-membrane structures, morphologically recognized as autophagosomes, had been reported in plants but had not been validated (Rose et al., 2006; Katsiarimpa et al., 2011; Reyes et al., 2011; Minibayeva et al., 2012). In our investigation, SH3P2-positive structures in *Arabidopsis* share several features with autophagosomes in mammalian cells: (1) They arise from the isolation membrane as well as from omegasome-like structures and subsequently wrap together into bi/multilayer-membrane autophagosome structures (Figures 4 and 5A; see Supplemental Figure 4 online); (2) they can expand and mature by fusing with endosomes or by engulfing cytoplasmic cargos (Figures 5B and 5C); and (3) they reacted positively with the autophagosome marker ATG8 (Figures 2, 6A, and 6C). All of these observations rendered SH3P2 a suitable indicator for autophagosome formation in *Arabidopsis*. Our description of autophagosome formation at the ultrastructural level is further supported by a dynamic analysis, in which we observed that autophagosome membranes elongate and bend into ring-like structures (Figure 3A).

We also demonstrated that the autophagosome membrane is likely derived from the ER membranes. It was previously reported in mammalian cells that the PAS assembly takes place on the ER membrane by forming a cup-shaped omegasome (Axe et al., 2008; Matsunaga et al., 2010; Tooze and Yoshimori,

Figure 9. (continued).

Phosphatidylethanolamine; PC, Phosphatidylcholine; S1P, Sphingosine 1-Phosphate; PtdIns(3,4)P2, Phosphatidylinositol (3,4) bisphosphate; PtdIns (3,5)P2, Phosphatidylinositol (3,5) bisphosphate; PtdIns(4,5)P2, Phosphatidylinositol (4,5) bisphosphate; PtdIns(3,4,5)P3, Phosphatidylinositol (3,4,5) trisphosphate; PA, Phosphatidic acid; PS, Phosphatidylserine.

(C) SH3P2 promotes PI3K foci formation. VPS34-GFP and ATG6-RFP were transiently expressed in *Arabidopsis* protoplasts together with CFP, SH3P2-CFP, or calnexin-SH3P2-CFP, respectively. Percentage of cells (>100) with punctae was quantified (right). Error bars represent the SD from three independent experiments. Bar = 50 μm.

(D) Wortmannin treatment suppresses the formation of SH3P2-GFP and mCherry-ATG8f compartments upon autophagy induction. Five-day-old double transgenic plants were subjected to autophagy induction with/without wortmannin treatment. Confocal images were collected after 5 h of treatment (right). Numbers of punctae per root section from different treatments were quantified (left). Error bars represent the SD from three independent experiments. Bar = 50 μm.

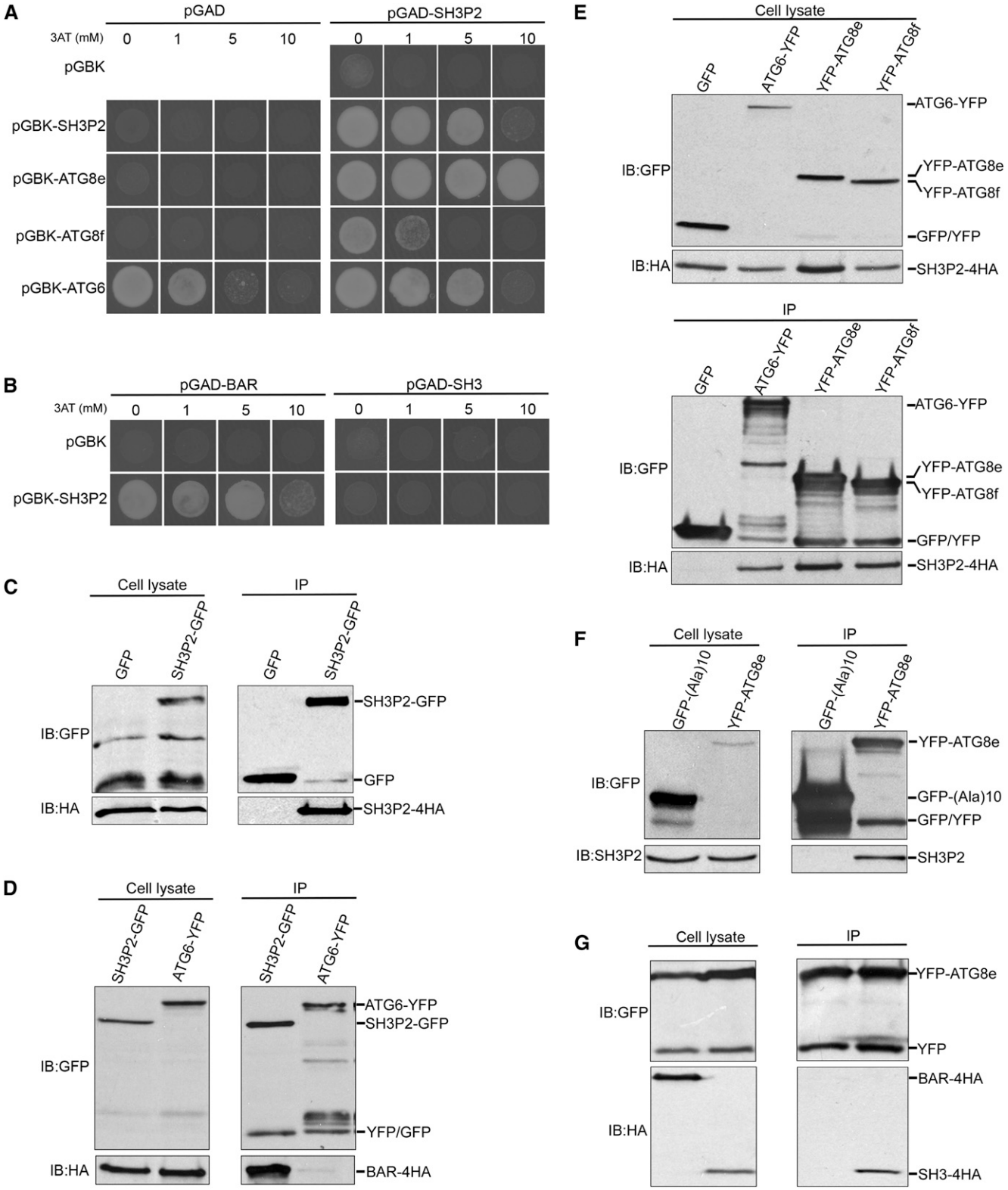

Figure 10. SH3P2 Associates with the PI3K Complex and Interacts with ATG8.

(A) Yeast two-hybrid analysis of the binary interactions between SH3P2 and the ATG proteins, ATG8e, ATG8f, and ATG6. 3AT (3-amino-1,2,4-triazole) was added and the corresponding concentrations were indicated at the top.

2010). This is also true in the closed form of SH3P2-positive structures, where the protruding ER membrane(s) and ER fragments were often detected outside and inside these structures, thus resembling the model of an omegasome intermediate (Figures 5A, 6B, and 6D; see Supplemental Figure 4B online). Such ER-associated structures have not previously been confirmed for autophagosome biogenesis in plants and are most likely to be the direct precursors of autophagosomes, as they were shown to mature into cup-shaped bi/multilayer structures. Accordingly, it is likely that SH3P2 translocates to the ER to facilitate the development of PAS during autophagy.

SH3P2 Is a Novel Membrane Binding Protein That Associates with the PI3K Complex during Autophagy in *Arabidopsis*

A key question related to autophagosome biogenesis is what the driving force is that achieves the membrane curvature necessary for the dynamic morphological changes during autophagy (Klionsky, 2005). Until now, no membrane-binding proteins that mediate autophagosome formation have been identified in plants. SH3P2 is structurally similar to Bif-1 (Figure 1A), which has been proposed to function as a membrane sensor through its BAR domain (Farsad et al., 2001; Takahashi et al., 2007, 2011, 2013). SH3P2 possesses a characteristic dimerization and membrane-binding ability, as evidenced by interaction studies and in vitro liposome/lipid binding assays (Figures 9A, 9B, and 10A to 10D). Particularly, SH3P2 is localized to the PAS and actively participates in membrane tubulation or fusion events during autophagosome formation (Figures 3 to 5; see Supplemental Movies 1 and 2 online).

Bif-1 has been shown to associate with the PI3K complex via UV radiation resistance-associated gene protein (Takahashi et al., 2007). We demonstrated that SH3P2 preferentially binds to PI3P, and SH3P2-GFP punctae are colocalized with PI3P-positive compartments (Figure 9B; see Supplemental Figure 6A online). We also observed that signals of SH3P2-GFP–positive punctae overlap with those of PI3K components (Figures 2A and 9C). Although a homolog of UV radiation resistance-associated gene protein remains to be identified in plants, our results support an indirect interaction between SH3P2 and the PI3K complex (Figures 10A and 10E). In addition, we have shown that SH3P2-GFP–positive punctae are significantly reduced in cells treated with the PI3K inhibitor wortmannin (Figure 9D), suggesting that SH3P2 functions as a downstream effector of the PI3K complex during autophagy. SH3P2 likely promotes expansion/maturation of the developing autophagosome membrane, which in turn may require recruiting more PI3K complex to PAS to generate PI3P. Accordingly, overexpression of SH3P2 facilitates the formation of ATG6-YFP and VPS34-GFP punctae, while this effect is suppressed when SH3P2 is anchored to the ER membrane (Figure 9C).

However, in contrast with Bif-1, knockdown of SH3P2 is lethal in plants (Figures 7A and 7C), while Bif-1 knockout mice grow normally but develop tumors in the tissues (Takahashi et al., 2007). Another notable discrepancy between SH3P2 and Bif-1 is that SH3P2 interacts with the ATG8 complex directly (Figures 10A and 10E to 10G). In addition, suppression of SH3P2 results in a higher level of ATG8e-PE (Figure 8D), whereas depletion of Bif-1 suppressed ATG8e-PE (Takahashi et al., 2007). Taken together, these results suggest that SH3P2 may function in a similar manner as Bif-1 but play a specific role in *Arabidopsis*.

SH3P2 Interacts with the ATG8 Complex and Is Required for Autophagosome Formation

In this study, we showed that SH3P2 knockdown impaired the autophagic pathway, in which the vacuolar delivery of YFP-ATG8e–positive structures was blocked, even in the presence of vacuole degradation inhibitors (Figures 8A and 8B). This scenario is further supported by the observation that downregulation of SH3P2 caused autophagosomes to accumulate and autophagic flux to be suppressed, as monitored by YFP-ATG8e/YFP and ATG8-PE, respectively (Figures 8C and 8D; see Supplemental Figure 5C online). However, the recruitment of YFP-ATG8e to the PAS is independent of SH3P2 activity (Figure 8A). These data together confirm that SH3P2 is required for autophagosome expansion/maturation.

Furthermore, we demonstrated that SH3P2 binds to both ATG8e and ATG8f via its C-terminal SH3 domain, which points to SH3P2 being a novel autophagy regulator in *Arabidopsis* (Figures 10A and 10E to 10G). This result is consistent with the recently proposed notion that the BAR-domain protein family may interact with ATG8 to promote PAS closure in plants (Li and

Figure 10. (continued).

(B) Yeast two-hybrid analysis of the binary interactions between SH3P2 and its truncation domains. 3AT was added and the corresponding concentrations are indicated at the top.

(C) Immunoprecipitation assay shows that SH3P2 has a self-interaction. Cell lysate from *Arabidopsis* PSBD protoplasts transiently expressing GFP/SH3P2-GFP and SH3P2-4HA for 12 h was subjected to a GFP trap assay. The resulting immunoprecipitation (IP) and cell lysate were analyzed by immunoblotting (IB) using anti-HA or anti-GFP antibodies.

(D) An immunoprecipitation assay shows that the BAR domain interacts with SH3P2 but not with ATG6. Cell lysate from *Arabidopsis* PSBD protoplasts transiently expressing ATG6-YFP or SH3P2-GFP together with BAR-4HA for 12 h were subjected to a GFP trap assay. The resulting immunoprecipitation and cell lysate were analyzed by immunoblotting using anti-HA or anti-GFP antibodies.

(E) SH3P2-4HA is precipitated with ATG6-GFP, YFP-ATG8e, and YFP-ATG8f. Plasmids were transiently expressed in *Arabidopsis* PSBD protoplasts for 12 h, and cell lysate was subjected to a GFP trap assay. The resulting immunoprecipitation and cell lysate were analyzed by immunoblotting using anti-HA and reprobed with anti-GFP antibodies.

(F) YFP-ATG8e interacts with endogenous SH3P2 in plants after autophagy induction. Cell lysate from 5-d-old GFP and YFP-ATG8e transgenic plants treated with BTH for 6 h and subjected to a GFP trap assay.

(G) SH3P2 requires the SH3 domain to interact with YFP-ATG8e.

Vierstra, 2012). Since SH3P2 has a membrane-remodeling domain, it is likely that an interaction between SH3P2 and ATG8 promotes membrane deformation for developing autophagosome. Recently, selective autophagy has been identified in plants, and the ATG8 family interacting motif has emerged as the molecular basis for ATG8 to recognize cargo(s) or other proteins in regulating autophagy (Suttangkakul et al., 2011; Svenning et al., 2011; Vanhee et al., 2011; Derrien et al., 2012; Floyd et al., 2012; Honig et al., 2012). Since SH3P2 signals were detected inside the vacuole after autophagy induction (Figures 1Bc and 1Bd), such an SH3P2-ATG8 interaction may target SH3P2 for degradation to regulate the turnover of autophagy.

However, unlike most ATG mutants reported in plants to date, which display relatively normal growth and only exhibit hypersensitivity to starvation conditions (Doelling et al., 2002; Hanaoka et al., 2002; Yoshimoto et al., 2004; Thompson et al., 2005; Phillips et al., 2008; Chung et al., 2010; Suttangkakul et al., 2011), knockdown of SH3P2 was developmentally lethal (Figures 7A and 7C). Considering the association between SH3P2 and the PI3K complex, our results fit well with findings from previous studies of the PI3K components, as all their knockout mutants result in lethality (Welters et al., 1994; Patel and Dinesh-Kumar, 2008; Xu et al., 2011). On the other hand, it is possible that SH3P2 has roles beyond autophagy. As the PI3K complex has been implicated in regulating both pollen germination and root hair growth in plants (Lee et al., 2008a, 2008b; Patel and Dinesh-Kumar, 2008), we indeed found that root hair growth is also impaired when SH3P2 is downregulated (Figure 7C). Future works should examine whether the lethality of the *sh3p2* mutant is due to its essential roles during autophagy or its involvement in other pathway(s).

Taken together, we have identified a novel non-ATG protein, SH3P2, which functions as an essential regulator of autophagy in *Arabidopsis*, and have provided direct evidence for the presumed model of membrane progression during autophagosome formation in plant cells. Regarding the membrane-tethering ability of SH3P2 and its association with the autophagy core machinery, we anticipate that future investigations of the molecular role of SH3P2 in membrane recruitment and remodeling will be crucial for unveiling the underlying mechanism of autophagosome biogenesis. This, in turn, will extend our understanding of the contribution of autophagy to more general aspects of plant development.

METHODS

Plasmid Construction

The GFP/YFP/RFP/mCherry/4HA fusion constructs used for transient expression in protoplasts were created by cloning the PCR-amplified cDNA into the pBI221 backbone containing the UBQ promoter. To generate the SH3P2 RNAi construct driven by 35S promoter, a 500-bp sequence of SH3P2 (nucleotide positions 477 to 976) predicted using MatchPoint (http://plantindustry.csiro.au/RNAi/software.htm) was amplified as two fragments and inserted into the hairpin RNAi vector pHANNIBAL (Helliwell and Waterhouse, 2005). The SH3P2 RNAi fragment was cloned downstream of a DEX-inducible promoter from pTA7002 (Aoyama and Chua, 1997). For recombinant protein expression, full-length SH3P2 was cloned into the pET-32a-c(+) (Novagen) or a modified pET3a-His-MBP vector (Chuck et al., 2011). Full-length ATG8e was cloned into pGEX4T (GE). The primers used to generate various corresponding constructs are listed in Supplemental Table 1 online. All constructs were confirmed by restriction mapping and DNA sequencing. The primers used in this study are listed in Supplemental Table 1 online.

Plant Materials and Growth and Treatment Conditions

To generate the transgenic plants, all the resulting constructs were introduced into *Agrobacterium tumefaciens* and transformed into wild-type Columbia-0 by floral dip (Clough and Bent, 1998). The GFP transgenic line was generated using the pEGAD plasmid (Cutler et al., 2000). To generate the double transgenic line, ER-mCherry (Basta-resistant) (Nelson et al., 2007) or mCherry-ATG8f (hygromycin-resistant) transgenic plants were first generated and then crossed into the SH3P2-GFP (kanamycin resistant) transgenic plant, respectively. T1 generations were screened with kanamycin and Basta/hygromycin for the presence of ER-mCherry or mCherry-ATG8e, respectively, and by fluorescence microscopy for red signal. For the UBQ:YFP-ATG8e/dex:RNAi-sh3p2 transgenic line, YFP-ATG8e (kanamycin-resistant) transgenic plants were crossed with *dex:RNAi-sh3p2* (hygromycin-resistant) transgenic plants, and the T1 generation was selected with kanamycin and hygromycin, followed by screening with the presence of YFP by fluorescence microscopy. Seeds were surface sterilized and sown on plates with Murashige and Skoog (MS) salts plus 0.8% agar. The seeded plates were kept at 4°C for 3 d before being moved to the growth chamber. The plates were incubated at 22°C under a long-day (16 h light/8 h dark) photoperiod. Plants exposed to long-day conditions were transferred to soil after 2 weeks. For starvation induction, 5-d-old seedlings were grown in liquid MS with methanol (1:100) as control or 100 μM BTH at least for 6 h prior to observation or as indicated. N starvation was performed by transferring the seedlings to MS or nitrogen-free MS plates for the indicated times. PI3K activity was inhibited by the addition of 8.95 μM wortmannin in the medium. To analyze the *dex:RNAi-sh3p2* plants, 7-d-old RNAi plants were transferred to MS plates supplemented with DEX (30 μM) for 2 d before other treatment.

Transient Expression in Protoplasts and Confocal Imaging

Transient expression in *Arabidopsis thaliana* plant system biology dark-type culture (PSBD) protoplasts was performed essentially as described previously (Miao and Jiang, 2007). Confocal fluorescence images were acquired 16 to 18 h after transformation using an Olympus FV1000 system. For each experiment or construct, more than 30 individual cells were observed for confocal imaging that represented >75% of the cells showing similar expression levels and patterns. Images were processed using Adobe Photoshop software (http://www.adobe.com) as previously described (Jiang and Rogers, 1998).

Antibodies

Antibodies against SH3P2 were generated with 6XHis-SH3P2 recombinant proteins as antigen. Recombinant 6XHis-SH3P2 proteins were purified from insoluble fractions as His fusion proteins using a Ni column according to standard methods (GE). Following SDS-PAGE, gel pieces containing the recombinant proteins as identified by Coomassie Brilliant Blue staining were extracted and injected directly into rabbits and rats at the Chinese University of Hong Kong. For anti-ATG8e antibody, GST (glutathione *S*-transferase)-ATG8e recombinant proteins were purified on a GST column (GE) following thrombin digestion. The resulting protein fragments were separated by SDS-PAGE following extraction and used as antigen for rat injection. Antibodies from the rabbits (SH3P2) or rats (ATG8e) were affinity purified using Cyanogen bromide–activated sepharose (Sigma-Aldrich) conjugated with recombinant proteins.

Lipid Binding and Liposome Flotation Assay

Both His-MBP-SH3P2 and His-MBP were expressed in *Escherichia coli* SoluBL21 cells upon induction with 0.4 mM isopropyl β-D-1-thiogalactopyranoside for 16 h at 28°C, followed by purification as His tag proteins using the His Spin Trap Kit (GE). The PIP strips/arrays (P-6001/6100; Echelon Biosciences) were blocked in 1% fat-free milk in TBS-T (Tris-buffered saline with Tween: 10 mM Tris-HCl, pH 8.0, 150 mM NaCl, and 0.1% Tween 20) at room temperature for 1 h. The strips/arrays were then incubated with 10 μg/mL of recombinant proteins at room temperature for 2 h. After incubation with proteins, the strips were washed three times in TBS-T and then incubated for 1 h with 1:100 mouse anti-His antibody (Santa Cruz Biotechnology) at room temperature, followed by three more washes in TBS-T. The signals were detected following the ECL Plus immunoblot method. For the liposome flotation assay, liposomes were prepared as described previously (Guo et al., 2013). Five micrograms of His-MBP-SH3P2 or His-MBP proteins was incubated with 8 μL of 1.8 mg/mL of liposomes in HKM buffer (20 mM HEPES, pH 7.4, 100 mM KCl, and 5 mM $MgCl_2$) containing 100 μM nucleotides at room temperature. The reaction mixture was adjusted to 1.75 M Suc and overlaid with 100 μL of 0.75 M Suc and 30 μL of HKM (20 mM HEPES, pH 7.4, 100 mM KCl, and 5 mM $MgCl_2$) buffer. The samples were centrifuged at 55,000 rpm in a TLS55 rotor in a Beckman ultracentrifuge for 2.5 h at 4°C. Fractions were collected from the bottom of the tube using a peristaltic pump (RAININ), and aliquots were analyzed by SDS-PAGE.

Confocal Immunofluorescence Studies

Fixation of root tips of 5-d-old seedlings and their subsequent labeling as well as their analysis by confocal immunofluorescence microscopy followed previously described methods (Jiang and Rogers, 1998; Lam et al., 2007). The settings for collecting confocal images within the linear range were as described (Jiang and Rogers, 1998). Antibodies were incubated at 4°C overnight at 4-μg/mL working concentrations. All confocal fluorescence images were collected using an Olympus FluoView FV1000 system. Images were processed using Adobe Photoshop software as previously described (Jiang and Rogers, 1998).

EM Studies of Resin-Embedded Cells

The general procedures used to prepare transmission EM samples and ultrathin sectioning of samples were described previously (Ritzenthaler et al., 2002; Tse et al., 2004). For high-pressure freezing, 5-d-old transgenic SH3P2-GFP root tips incubated with/without BTH treatment in MS for 6 h were cut from the seedlings and immediately frozen in a high-pressure freezing apparatus (EM PACT2; Leica), with subsequent freeze substitution in dry acetone containing 0.1% uranyl acetate at −85°C. Infiltration with Lowicryl HM20 (Electron Microscopy Sciences), embedding, and UV polymerization were performed stepwise at −35°C. For immunolabeling, standard procedures were performed as described previously (Lam et al., 2007). The working concentration of affinity-purified antibodies was 40 μg/mL. Calnexin antibodies (Agrisera) were used at a dilution of 1:100. Gold particle–coupled secondary antibodies were diluted as 1:40, followed by a poststaining procedure using aqueous uranyl acetate/lead citrate. Sections were examined using a Hitachi H-7650 transmission electron microscope with a charge-coupled device camera operating at 80 kV (Hitachi High-Technologies).

RT-PCR

RNA was isolated from plate-grown plants subjected to the indicated treatment (Invitrogen). The first strand for each cDNA was synthesized by Superscript II reverse transcriptase (Invitrogen) in combination with the reverse primer P25 described in Supplemental Table 1 online. Thirty cycles of RT-PCR were then performed using this template, GoTaq polymerase (Bio-Rad), and the reverse primers in combination with forward primers (see Supplemental Table 1 online). The actin gene was used as a RT-PCR internal control.

Protein Extraction and Immunoblot Analysis

To prepare cell extracts from protoplasts, transformed protoplasts were first diluted threefold with 250 mM NaCl and then harvested by centrifugation at 100*g* for 10 min, followed by resuspension in lysis buffer containing 25 mM Tris-HCl, pH 7.5, 150 mM NaCl, 1 mM EDTA, 1% SDS, and 1× Complete Protease Inhibitor Cocktail (Roche). The total cell extracts were centrifuged at 20,000*g* for 30 min at 4°C. For plants, 5-d-old seedlings were ground in liquid nitrogen and extracted with the lysis buffer mentioned above, following the SDS-PAGE or analyzed by immunoblotting. For immunoblot analysis, mouse hemagglutinin antibodies (Abcam) were used at a dilution of 1:1000, while 4 μg/mL of purified antibodies was used and rat serum was diluted by 1:100. Quantification of the relative gray-scale intensity in immunoblot analysis was done using ImageJ software v1.45 (http://lukemiller.org/index.php/2010/11/analyzing-gels-and-western-blots-with-image-j/).

Yeast Two-Hybrid Analysis

Yeast-two hybrid analysis was performed using the MatchMaker GAL4 Two-Hybrid System 3 (Clontech) according to the manufacturer's instructions. The cDNAs were cloned into the pGBKT7 and pGADT7 vectors (Clontech). Pairs of pGBKT7 and pGADT7 vectors were cotransformed into the *Saccharomyces cerevisiae* strain AH109. Diploids were selected on synthetic drop-out (SD) medium lacking Trp and Leu (SD-TrpLeu), while the selection of yeast cells expressing interacting proteins was made on SD medium lacking His, Trp, and Leu (SD-His-Trp-Leu) containing 0 to 10 mM 3-AT (3-amino-1,2,4-triazole). The experiments (yeast transformation, mating, and selection) were repeated several times independently and similar results were obtained.

Immunoprecipitations

Protein extraction and immunoprecipitation were performed as described with some modifications (Cai et al., 2012). Total cell lysates were prepared in lysis buffer (10 mM Tris/HCl at pH 7.4, 150 mM NaCl, 0.5 mM EDTA, 5% glycerol, 0.2% Nonidet P-40, and 2 mM dithiobis [succinimidyl propionate] containing 1× Complete Protease Inhibitor Cocktail) and were then incubated with GFP-TRAP agarose beads (ChromoTek) overnight at 4°C. Samples were washed five times (2000*g*, 1 min, 4°C) in wash buffer (10 mM Tris/HCl, pH 7.5, 150 mM NaCl, and 0.5 mM EDTA with 1× Complete Protease Inhibitor Cocktail) and then eluted by boiling in 2× SDS sample buffer. Samples were separated by SDS-PAGE and analyzed by immunoblot using appropriate antibodies.

Accession Numbers

The Arabidopsis Genome Initiative locus identifiers for the genes mentioned in this article are as follows: SH3P1 (AT1G31440), SH3P2 (AT4G34660), SH3P3 (AT4G18060), VPS34 (AT1G60490), ATG6 (AT3G61710), ATG8e (AT2G45170), ATG8f (AT4G16520), and ATG9 (AT2G31260).

Supplemental Data

The following materials are available in the online version of this article.

Supplemental Figure 1. Sequence Alignment for SH3P2.

Supplemental Figure 2. Time-Course Analysis of the Response of SH3P2-GFP to Autophagy Induction and Characterization of ATG8e Antibodies.

Supplemental Figure 3. Confocal Analysis of the Subcellular Localization of SH3P1, SH3P2, SH3P3 and Relationship between SH3P2 and Conventional Organelle Markers in Transient Expressed *Arabidopsis* PSBD Protoplasts.

Supplemental Figure 4. Immuno-EM Analysis of SH3P2-GFP–Positive Organelles with GFP Antibodies and Their Connection with the ER Membrane.

Supplemental Figure 5. Characterization of *dex*:*RNAi-sh3p2* Plants.

Supplemental Figure 6. Confocal Analysis of the Relationship between SH3P2-Containing Compartments and PI3P and the Effect of CNX-SH3P2-CFP.

Supplemental Table 1. Oligonucleotides Used in This Study.

Supplemental Movie 1. An Overview of Autophagosome Formation Labeled by SH3P2-GFP in the SH3P2-GFP Transgenic Root Tip Cells after BTH Treatment for 8 h.

Supplemental Movie 2. Dynamics of the Tubular Structures Labeled by SH3P2-GFP in the SH3P2-GFP Transgenic Root Tip Cells after BTH Treatment for 8 h.

ACKNOWLEDGMENTS

We thank Randy W. Schekman (University of California at Berkeley) for support with the liposome binding experiment. This work was partially supported by grants from the Research Grants Council of Hong Kong (CUHK466610, CUHK466011, CUHK465112, CUHK2/CRF/11G, and HKUST10/CRF/12R), the National Natural Science Foundation of China/Research Grants Council (N_CUHK406/12), the National Natural Science Foundation of China (31270226), Shenzhen Basic Research Project (JCYJ20120619150052041), and the Shenzhen Peacock Project (KQTD201101; to L.J.). S.K.L. is supported by a Human Frontier Science Program Long-Term Fellowship.

AUTHOR CONTRIBUTIONS

X.Z. and L.J. conceived and designed the experiments. X.Z., H.W., S.K.L., and C.G. performed the experiments. X.Z., H.W., C.G., X.W., and Y.C. analyzed the data. X.Z. and L.J. wrote the article.

Received September 6, 2013; revised September 6, 2013; accepted October 21, 2013; published November 18, 2013.

REFERENCES

Arabidopsis Interactome Mapping Consortium (2011). Evidence for network evolution in an *Arabidopsis* interactome map. Science **333:** 601–607.

Aoyama, T., and Chua, N.H. (1997). A glucocorticoid-mediated transcriptional induction system in transgenic plants. Plant J. **11:** 605–612.

Avin-Wittenberg, T., Honig, A., and Galili, G. (2012). Variations on a theme: Plant autophagy in comparison to yeast and mammals. Protoplasma **249:** 285–299.

Axe, E.L., Walker, S.A., Manifava, M., Chandra, P., Roderick, H.L., Habermann, A., Griffiths, G., and Ktistakis, N.T. (2008). Autophagosome formation from membrane compartments enriched in phosphatidylinositol 3-phosphate and dynamically connected to the endoplasmic reticulum. J. Cell Biol. **182:** 685–701.

Blommaart, E.F., Krause, U., Schellens, J.P., Vreeling-Sindelárová, H., and Meijer, A.J. (1997). The phosphatidylinositol 3-kinase inhibitors wortmannin and LY294002 inhibit autophagy in isolated rat hepatocytes. Eur. J. Biochem. **243:** 240–246.

Cai, Y., Zhuang, X., Wang, J., Wang, H., Lam, S.K., Gao, C., Wang, X., and Jiang, L. (2012). Vacuolar degradation of two integral plasma membrane proteins, AtLRR84A and OsSCAMP1, is cargo ubiquitination-independent and prevacuolar compartment-mediated in plant cells. Traffic **13:** 1023–1040.

Chuck, C.P., Chow, H.F., Wan, D.C., and Wong, K.B. (2011). Profiling of substrate specificities of 3C-like proteases from group 1, 2a, 2b, and 3 coronaviruses. PLoS ONE **6:** e27228.

Chung, T., Phillips, A.R., and Vierstra, R.D. (2010). ATG8 lipidation and ATG8-mediated autophagy in *Arabidopsis* require ATG12 expressed from the differentially controlled ATG12A and ATG12B loci. Plant J. **62:** 483–493.

Clough, S.J., and Bent, A.F. (1998). Floral dip: A simplified method for Agrobacterium-mediated transformation of *Arabidopsis thaliana*. Plant J. **16:** 735–743.

Contento, A.L., Xiong, Y., and Bassham, D.C. (2005). Visualization of autophagy in *Arabidopsis* using the fluorescent dye monodansylcadaverine and a GFP-AtATG8e fusion protein. Plant J. **42:** 598–608.

Cutler, S.R., Ehrhardt, D.W., Griffitts, J.S., and Somerville, C.R. (2000). Random GFP:cDNA fusions enable visualization of subcellular structures in cells of *Arabidopsis* at a high frequency. Proc. Natl. Acad. Sci. USA **97:** 3718–3723.

daSilva, L.L., Foresti, O., and Denecke, J. (2006). Targeting of the plant vacuolar sorting receptor BP80 is dependent on multiple sorting signals in the cytosolic tail. Plant Cell **18:** 1477–1497.

Dawson, J.C., Legg, J.A., and Machesky, L.M. (2006). Bar domain proteins: A role in tubulation, scission and actin assembly in clathrin-mediated endocytosis. Trends Cell Biol. **16:** 493–498.

Derrien, B., Baumberger, N., Schepetilnikov, M., Viotti, C., De Cillia, J., Ziegler-Graff, V., Isono, E., Schumacher, K., and Genschik, P. (2012). Degradation of the antiviral component ARGONAUTE1 by the autophagy pathway. Proc. Natl. Acad. Sci. USA **109:** 15942–15946.

Doelling, J.H., Walker, J.M., Friedman, E.M., Thompson, A.R., and Vierstra, R.D. (2002). The APG8/12-activating enzyme APG7 is required for proper nutrient recycling and senescence in *Arabidopsis thaliana*. J. Biol. Chem. **277:** 33105–33114.

Farsad, K., Ringstad, N., Takei, K., Floyd, S.R., Rose, K., and De Camilli, P. (2001). Generation of high curvature membranes mediated by direct endophilin bilayer interactions. J. Cell Biol. **155:** 193–200.

Floyd, B.E., Morriss, S.C., Macintosh, G.C., and Bassham, D.C. (2012). What to eat: Evidence for selective autophagy in plants. J. Integr. Plant Biol. **54:** 907–920.

Frost, A., Unger, V.M., and De Camilli, P. (2009). The BAR domain superfamily: Membrane-molding macromolecules. Cell **137:** 191–196.

Fujiki, Y., Yoshimoto, K., and Ohsumi, Y. (2007). An Arabidopsis homolog of yeast ATG6/VPS30 is essential for pollen germination. Plant Physiol. **143:** 1132–1139.

Ge, L., Melville, D., Zhang, M., and Schekman, R. (2013). The ER-Golgi intermediate compartment is a key membrane source for the LC3 lipidation step of autophagosome biogenesis. Elife **2:** e00947.

Guo, Y., Zanetti, G., and Schekman, R. (2013). A novel GTP-binding protein-adaptor protein complex responsible for export of Vangl2 from the trans Golgi network. Elife **2:** e00160.

Hailey, D.W., Rambold, A.S., Satpute-Krishnan, P., Mitra, K., Sougrat, R., Kim, P.K., and Lippincott-Schwartz, J. (2010). Mitochondria supply membranes for autophagosome biogenesis during starvation. Cell **141:** 656–667.

Hamasaki, M., Furuta, N., Matsuda, A., Nezu, A., Yamamoto, A., Fujita, N., Oomori, H., Noda, T., Haraguchi, T., Hiraoka, Y.,

Amano, A., and Yoshimori, T. (2013). Autophagosomes form at ER-mitochondria contact sites. Nature **495:** 389–393.

Hanamata, S., Kurusu, T., Okada, M., Suda, A., Kawamura, K., Tsukada, E., and Kuchitsu, K. (2012). In vivo imaging and quantitative monitoring of autophagic flux in tobacco BY-2 cells. Plant Signal. Behav. **8:** e22510.

Hanaoka, H., Noda, T., Shirano, Y., Kato, T., Hayashi, H., Shibata, D., Tabata, S., and Ohsumi, Y. (2002). Leaf senescence and starvation-induced chlorosis are accelerated by the disruption of an Arabidopsis autophagy gene. Plant Physiol. **129:** 1181–1193.

Hayashi-Nishino, M., Fujita, N., Noda, T., Yamaguchi, A., Yoshimori, T., and Yamamoto, A. (2010a). Electron tomography reveals the endoplasmic reticulum as a membrane source for autophagosome formation. Autophagy **6:** 301–303.

Hayashi-Nishino, M., Fujita, N., Noda, T., Yamaguchi, A., Yoshimori, T., and Yamamoto, A. (2010b). A subdomain of the endoplasmic reticulum forms a cradle for autophagosome formation. Nat. Cell Biol. **11:** 1433–1437.

Helling, D., Possart, A., Cottier, S., Klahre, U., and Kost, B. (2006). Pollen tube tip growth depends on plasma membrane polarization mediated by tobacco PLC3 activity and endocytic membrane recycling. Plant Cell **18:** 3519–3534.

Helliwell, C.A., and Waterhouse, P.M. (2005). Constructs and methods for hairpin RNA-mediated gene silencing in plants. Methods Enzymol. **392:** 24–35.

Honig, A., Avin-Wittenberg, T., Ufaz, S., and Galili, G. (2012). A new type of compartment, defined by plant-specific Atg8-interacting proteins, is induced upon exposure of *Arabidopsis* plants to carbon starvation. Plant Cell **24:** 288–303.

Jiang, L., and Rogers, J.C. (1998). Integral membrane protein sorting to vacuoles in plant cells: Evidence for two pathways. J. Cell Biol. **143:** 1183–1199.

Katsiarimpa, A., Anzenberger, F., Schlager, N., Neubert, S., Hauser, M.T., Schwechheimer, C., and Isono, E. (2011). The *Arabidopsis* deubiquitinating enzyme AMSH3 interacts with ESCRT-III subunits and regulates their localization. Plant Cell **23:** 3026–3040.

Klionsky, D.J. (2005). The molecular machinery of autophagy: Unanswered questions. J. Cell Sci. **118:** 7–18.

Lam, B.C., Sage, T.L., Bianchi, F., and Blumwald, E. (2001). Role of SH3 domain-containing proteins in clathrin-mediated vesicle trafficking in *Arabidopsis*. Plant Cell **13:** 2499–2512.

Lam, B.C., Sage, T.L., Bianchi, F., and Blumwald, E. (2002). Regulation of ADL6 activity by its associated molecular network. Plant J. **31:** 565–576.

Lam, S.K., Siu, C.L., Hillmer, S., Jang, S., An, G., Robinson, D.G., and Jiang, L. (2007). Rice SCAMP1 defines clathrin-coated, trans-golgi-located tubular-vesicular structures as an early endosome in tobacco BY-2 cells. Plant Cell **19:** 296–319.

Lee, Y., Bak, G., Choi, Y., Chuang, W.I., Cho, H.T., and Lee, Y. (2008a). Roles of phosphatidylinositol 3-kinase in root hair growth. Plant Physiol. **147:** 624–635.

Lee, Y., Kim, E.S., Choi, Y., Hwang, I., Staiger, C.J., Chung, Y.Y., and Lee, Y. (2008b). The Arabidopsis phosphatidylinositol 3-kinase is important for pollen development. Plant Physiol. **147:** 1886–1897.

Li, F., and Vierstra, R.D. (2012). Autophagy: A multifaceted intracellular system for bulk and selective recycling. Trends Plant Sci. **17:** 526–537.

Liu, Y., and Bassham, D.C. (2012). Autophagy: Pathways for self-eating in plant cells. Annu. Rev. Plant Biol. **63:** 215–237.

Liu, Y., Schiff, M., Czymmek, K., Tallóczy, Z., Levine, B., and Dinesh-Kumar, S.P. (2005). Autophagy regulates programmed cell death during the plant innate immune response. Cell **121:** 567–577.

Matsunaga, K., Morita, E., Saitoh, T., Akira, S., Ktistakis, N.T., Izumi, T., Noda, T., and Yoshimori, T. (2010). Autophagy requires endoplasmic reticulum targeting of the PI3-kinase complex via Atg14L. J. Cell Biol. **190:** 511–521.

Miao, Y., and Jiang, L. (2007). Transient expression of fluorescent fusion proteins in protoplasts of suspension cultured cells. Nat. Protoc. **2:** 2348–2353.

Minibayeva, F., Dmitrieva, S., Ponomareva, A., and Ryabovol, V. (2012). Oxidative stress-induced autophagy in plants: The role of mitochondria. Plant Physiol. Biochem. **59:** 11–19.

Mizushima, N., and Komatsu, M. (2011). Autophagy: Renovation of cells and tissues. Cell **147:** 728–741.

Mizushima, N., Yoshimori, T., and Levine, B. (2010). Methods in mammalian autophagy research. Cell **140:** 313–326.

Mizushima, N., Yoshimori, T., and Ohsumi, Y. (2011). The role of Atg proteins in autophagosome formation. Annu. Rev. Cell Dev. Biol. **27:** 107–132.

Nelson, B.K., Cai, X., and Nebenführ, A. (2007). A multicolored set of in vivo organelle markers for co-localization studies in *Arabidopsis* and other plants. Plant J. **51:** 1126–1136.

Niemes, S., Labs, M., Scheuring, D., Krueger, F., Langhans, M., Jesenofsky, B., Robinson, D.G., and Pimpl, P. (2010). Sorting of plant vacuolar proteins is initiated in the ER. Plant J. **62:** 601–614.

Noda, T., Matsunaga, K., and Yoshimori, T. (2011). Atg14L recruits PtdIns 3-kinase to the ER for autophagosome formation. Autophagy **7:** 438–439.

Ohashi, Y., and Munro, S. (2010). Membrane delivery to the yeast autophagosome from the Golgi-endosomal system. Mol. Biol. Cell **21:** 3998–4008.

Patel, S., and Dinesh-Kumar, S.P. (2008). *Arabidopsis* ATG6 is required to limit the pathogen-associated cell death response. Autophagy **4:** 20–27.

Phillips, A.R., Suttangkakul, A., and Vierstra, R.D. (2008). The ATG12-conjugating enzyme ATG10 Is essential for autophagic vesicle formation in *Arabidopsis thaliana*. Genetics **178:** 1339–1353.

Ravikumar, B., Moreau, K., Jahreiss, L., Puri, C., and Rubinsztein, D.C. (2010). Plasma membrane contributes to the formation of pre-autophagosomal structures. Nat. Cell Biol. **12:** 747–757.

Reyes, F.C., Chung, T., Holding, D., Jung, R., Vierstra, R., and Otegui, M.S. (2011). Delivery of prolamins to the protein storage vacuole in maize aleurone cells. Plant Cell **23:** 769–784.

Ritzenthaler, C., Nebenführ, A., Movafeghi, A., Stussi-Garaud, C., Behnia, L., Pimpl, P., Staehelin, L.A., and Robinson, D.G. (2002). Reevaluation of the effects of brefeldin A on plant cells using tobacco Bright Yellow 2 cells expressing Golgi-targeted green fluorescent protein and COPI antisera. Plant Cell **14:** 237–261.

Rose, T.L., Bonneau, L., Der, C., Marty-Mazars, D., and Marty, F. (2006). Starvation-induced expression of autophagy-related genes in *Arabidopsis*. Biol. Cell **98:** 53–67.

Suttangkakul, A., Li, F., Chung, T., and Vierstra, R.D. (2011). The ATG1/ATG13 protein kinase complex is both a regulator and a target of autophagic recycling in *Arabidopsis*. Plant Cell **23:** 3761–3779.

Svenning, S., Lamark, T., Krause, K., and Johansen, T. (2011). Plant NBR1 is a selective autophagy substrate and a functional hybrid of the mammalian autophagic adapters NBR1 and p62/SQSTM1. Autophagy **7:** 993–1010.

Takahashi, Y., Coppola, D., Matsushita, N., Cualing, H.D., Sun, M., Sato, Y., Liang, C., Jung, J.U., Cheng, J.Q., Mulé, J.J., Pledger, W.J., and Wang, H.G. (2007). Bif-1 interacts with Beclin 1 through UVRAG and regulates autophagy and tumorigenesis. Nat. Cell Biol. **9:** 1142–1151.

Takahashi, Y., Hori, T., Cooper, T.K., Liao, J., Desai, N., Serfass, J.M., Young, M.M., Park, S., Izu, Y., and Wang, H.G. (2013). Bif-1 haploinsufficiency promotes chromosomal instability and accelerates Myc-driven lymphomagenesis via suppression of mitophagy. Blood **121:** 1622–1632.

Takahashi, Y., Meyerkord, C.L., Hori, T., Runkle, K., Fox, T.E., Kester, M., Loughran, T.P., and Wang, H.G. (2011). Bif-1 regulates Atg9 trafficking by mediating the fission of Golgi membranes during autophagy. Autophagy **7:** 61–73.

Takatsuka, C., Inoue, Y., Higuchi, T., Hillmer, S., Robinson, D.G., and Moriyasu, Y. (2011). Autophagy in tobacco BY-2 cells cultured under sucrose starvation conditions: Isolation of the autolysosome and its characterization. Plant Cell Physiol. **52:** 2074–2087.

Takatsuka, C., Inoue, Y., Matsuoka, K., and Moriyasu, Y. (2004). 3-Methyladenine inhibits autophagy in tobacco culture cells under sucrose starvation conditions. Plant Cell Physiol. **45:** 265–274.

Thole, J.M., Vermeer, J.E., Zhang, Y., Gadella, T.W., Jr., and Nielsen, E. (2008). Root hair defective4 encodes a phosphatidylinositol-4-phosphate phosphatase required for proper root hair development in *Arabidopsis thaliana*. Plant Cell **20:** 381–395.

Thompson, A.R., Doelling, J.H., Suttangkakul, A., and Vierstra, R.D. (2005). Autophagic nutrient recycling in Arabidopsis directed by the ATG8 and ATG12 conjugation pathways. Plant Physiol. **138:** 2097–2110.

Thompson, A.R., and Vierstra, R.D. (2005). Autophagic recycling: Lessons from yeast help define the process in plants. Curr. Opin. Plant Biol. **8:** 165–173.

Tooze, S.A., and Yoshimori, T. (2010). The origin of the autophagosomal membrane. Nat. Cell Biol. **12:** 831–835.

Toyooka, K., Moriyasu, Y., Goto, Y., Takeuchi, M., Fukuda, H., and Matsuoka, K. (2006). Protein aggregates are transported to vacuoles by a macroautophagic mechanism in nutrient-starved plant cells. Autophagy **2:** 96–106.

Tse, Y.C., Mo, B., Hillmer, S., Zhao, M., Lo, S.W., Robinson, D.G., and Jiang, L. (2004). Identification of multivesicular bodies as prevacuolar compartments in *Nicotiana tabacum* BY-2 cells. Plant Cell **16:** 672–693.

Vanhee, C., Zapotoczny, G., Masquelier, D., Ghislain, M., and Batoko, H. (2011). The *Arabidopsis* multistress regulator TSPO is a heme binding membrane protein and a potential scavenger of porphyrins via an autophagy-dependent degradation mechanism. Plant Cell **23:** 785–805.

Vermeer, J.E., van Leeuwen, W., Tobeña-Santamaria, R., Laxalt, A.M., Jones, D.R., Divecha, N., Gadella, T.W., Jr., and Munnik, T. (2006). Visualization of PtdIns3P dynamics in living plant cells. Plant J. **47:** 687–700.

Wang, H., Zhuang, X., Cai, Y., Cheung, A.Y., and Jiang, L. (2013). Apical F-actin-regulated exocytic targeting of NtPPME1 is essential for construction and rigidity of the pollen tube cell wall. Plant J. **76:** 367–379.

Wang, Y., Nishimura, M.T., Zhao, T., and Tang, D. (2011). ATG2, an autophagy-related protein, negatively affects powdery mildew resistance and mildew-induced cell death in *Arabidopsis*. Plant J. **68:** 74–87.

Welters, P., Takegawa, K., Emr, S.D., and Chrispeels, M.J. (1994). AtVPS34, a phosphatidylinositol 3-kinase of *Arabidopsis thaliana*, is an essential protein with homology to a calcium-dependent lipid binding domain. Proc. Natl. Acad. Sci. USA **91:** 11398–11402.

Xie, Z., and Klionsky, D.J. (2007). Autophagosome formation: Core machinery and adaptations. Nat. Cell Biol. **9:** 1102–1109.

Xu, N., Gao, X.Q., Zhao, X.Y., Zhu, D.Z., Zhou, L.Z., and Zhang, X.S. (2011). *Arabidopsis* AtVPS15 is essential for pollen development and germination through modulating phosphatidylinositol 3-phosphate formation. Plant Mol. Biol. **77:** 251–260.

Yoshimoto, K., Hanaoka, H., Sato, S., Kato, T., Tabata, S., Noda, T., and Ohsumi, Y. (2004). Processing of ATG8s, ubiquitin-like proteins, and their deconjugation by ATG4s are essential for plant autophagy. Plant Cell **16:** 2967–2983.

Yoshimoto, K., Jikumaru, Y., Kamiya, Y., Kusano, M., Consonni, C., Panstruga, R., Ohsumi, Y., and Shirasu, K. (2009). Autophagy negatively regulates cell death by controlling NPR1-dependent salicylic acid signaling during senescence and the innate immune response in *Arabidopsis*. Plant Cell **21:** 2914–2927.

Zhang, Y., Li, S., Zhou, L.Z., Fox, E., Pao, J., Sun, W., Zhou, C., and McCormick, S. (2011). Overexpression of *Arabidopsis thaliana* PTEN caused accumulation of autophagic bodies in pollen tubes by disrupting phosphatidylinositol 3-phosphate dynamics. Plant J. **68:** 1081–1092.